AFRL-AFOSR-VA-TR-2022-0100

Non-Hermitian and Open Systems: Form Fundamentals to Applications

Kolesik, Miroslav
UNIVERSITY OF ARIZONA
888 N EUCLID AVE RM 510
TUCSON, AZ, 85719
USA

02/09/2022
Final Technical Report

Air Force Research Laboratory
Air Force Office of Scientific Research
Arlington, Virginia 22203
Air Force Materiel Command

REPORT DOCUMENTATION PAGE

PLEASE DO NOT RETURN YOUR FORM TO THE ABOVE ORGANIZATION.

1. REPORT DATE	2. REPORT TYPE	3. DATES COVERED	
		START DATE	END DATE
20220209	Final	20180615	20211031

4. TITLE AND SUBTITLE
Non-Hermitian and Open Systems: Form Fundamentals to Applications

5a. CONTRACT NUMBER	5b. GRANT NUMBER	5c. PROGRAM ELEMENT NUMBER
	FA9550-18-1-0183	61102F
5d. PROJECT NUMBER	**5e. TASK NUMBER**	**5f. WORK UNIT NUMBER**

6. AUTHOR(S)
Miroslav Kolesik

7. PERFORMING ORGANIZATION NAME(S) AND ADDRESS(ES)
UNIVERSITY OF ARIZONA
888 N EUCLID AVE RM 510
TUCSON, AZ 85719
USA

8. PERFORMING ORGANIZATION REPORT NUMBER

9. SPONSORING/MONITORING AGENCY NAME(S) AND ADDRESS(ES)	10. SPONSOR/MONITOR'S ACRONYM(S)	11. SPONSOR/MONITOR'S REPORT NUMBER(S)
Air Force Office of Scientific Research 875 N. Randolph St. Room 3112 Arlington, VA 22203	AFRL/AFOSR RTB1	AFRL-AFOSR-VA-TR-2022-0100

12. DISTRIBUTION/AVAILABILITY STATEMENT
A Distribution Unlimited: PB Public Release

13. SUPPLEMENTARY NOTES

14. ABSTRACT
The project investigated non-Hermitian and open systems in the field of optical physics. New algorithms were developed to calculate meta-stable states in atoms and/or molecules, enabling the construction of the model for the nonlinear properties of molecular oxygen. This completed the set of models utilizing Metastable Electronic State Approach, and was applied to the large-scale modeling of long-wavelength infrared pulses propagating nonlinearly through atmospheric turbulence. Non-Hermitian methods were applied to the electron emission from metallic nano-structures, leading to the prediction of a new source of nonlinear optical polarization. Time-resolved dynamics of quantum tunneling was studied in several systems, including atoms an metallic structures, shedding light on the currently open question of tunneling time. Universality of the nonlinear optical response of atoms was identified and applied to improve numerical modeling in NLO.

15. SUBJECT TERMS

16. SECURITY CLASSIFICATION OF:			17. LIMITATION OF ABSTRACT	18. NUMBER OF PAGES
a. REPORT	b. ABSTRACT	c. THIS PAGE		
U	U	U	UU	41

19a. NAME OF RESPONSIBLE PERSON	19b. PHONE NUMBER *(Include area code)*
ARJE NACHMAN	426-8427

Contract/Grant Title:

Non-Hermitian and Open Systems: Form Fundamentals to Applications

Contract/Grant #: FA9550-18-1-0183

Principal investigator: Miroslav Kolesik

AFOSR program manager: Dr. Arje Nachman

Period of performance: Jun 15, 2018 through October 31, 2021

Submission date: 20 Jan. 2022

Publicly Releasable

Contents

1 Accomplishments **3**
1.1 Mathematics and numerical algorithms for open and non-Hermitian systems 3
1.1.1 Universal long-wavelength nonlinear optical response 3
1.1.2 Stark resonances as a complete basis for open quantum systems 5
1.1.3 Computational boundary conditions for open systems 6
1.1.4 Quantum-tunneling dynamics 8
1.1.5 Exact continuum eigenstates of the Stark-Coulomb Hamiltonian 10
1.1.6 Continuum-energy Stark-Coulomb basis 11
1.1.7 Exact time-dependent description of a tunneling electron 13
1.1.8 Impact and future applications 14
1.1.9 Connecting quantum and classical description in quantum tunneling 15
1.2 Metallic nano-structures exposed to strong field 17
1.2.1 Generalization of the Fowler-Nordheim approach 17
1.2.2 Nonlinear polarization and high-harmonic radiation from metallic nano-tips . 18
1.3 Extreme nonlinear optics with Metastable Electronic State Method 20
1.3.1 Utilizing universality and experiments to calibrate optical nonlinear response 20
1.3.2 Post-Kerr-like optical-response nonlinearity 22
1.3.3 Meta-stable electronic states in multi-electron systems: Molecular oxygen . . 23
1.3.4 Turbulence and nonlinearity in LWIR 26
1.3.5 Laser-acceleration of electrons 28
1.3.6 Broad-band high-intensity pulse propagation for efficient high-harmonic generation 29

2 Impacts **31**
2.1 Primary discipline (broadly defined light-matter interactions) 31
2.1.1 Broadening the application field of non-Hermitian approaches 31
2.1.2 New exactly solvable models 31
2.1.3 Addressing fundamental questions of light matter interactions 32
2.1.4 Novel numerical methods 33
2.1.5 Extensions of MESA to multielectron systems 33
2.1.6 Simulation tools for large-scale simulations of LWIR pulses in atmosphere . 33
2.1.7 New exact results for an ubiquitous quantum Hamiltonian 34
2.2 Outreach work related to the project 34
2.3 Graduate education 35
2.4 Collaborations and synergy with other projects 35

3 Dissemination of Results:
Archival Publications, Invited Talks, Conference Contributions **36**

4 References **38**

5 Changes **41**

6 Technical updates **41**

1 Accomplishments

Because there are several complementary lines of research, the results in this report are grouped into topics, rather then following an ordered time-line. We start with our more mathematical work, where the emphasis is on exact results for solvable models and/or or physical predictions which are based on mathematical analysis of model systems. Then we continue with algorithmic and implementation problems, and follow up with "applications" and description of our collaborative research in which the results of this effort played a central role.

1.1 Mathematics and numerical algorithms for open and non-Hermitian systems

1.1.1 Universal long-wavelength nonlinear optical response

The concept of universality plays an important role in a wide range of physical systems. Reflecting the fact that certain behaviors of a system are independent of specific details, it provides a powerful tool to understand the common properties of different systems in a unified way. The concept is best known from statistical mechanics where classes of systems display detail-independent properties [1,2].

One of our projects dealt with the extension of the universality concept to the description of the optical nonlinearity and ionization in long-wavelength optical fields (publication P6). We have demonstrated numerically (and provided a qualitative justification) that the long-wavelength nonlinear dipole moment and ionization rate versus electric field strength F for different noble gases can be described in a unified way. Namely, as is illustrated in the following Fig.1, they can be scaled onto each other, by changing or stretching axes of the electric field-strength and of the nonlinear response be it the induced dipole moment or the ionization rate caused by the external field.

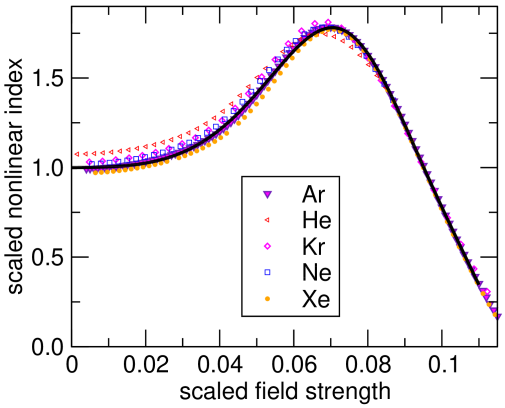

Figure 1: Collapse of the nonlinear dipole-moment curves in noble gases onto a single universal form $M(\mathcal{F})/M(0)$ versus scaled field strength $\mathcal{F} = \beta_a F$ with β_a standing for species-specific scaling parameter (please see text). The numerical data based on ssMESA for each atomic species is shown by the various symbols, while the solid line represents a universal master, or scaling function.

In doing so, we were able to reveal universal functions that characterize the form of the nonlinear response. These "master functions" express the scaling properties of the imaginary part of the resonant energy Γ and of the nonlinear dipole moment p_{nl} as functions of the external field strength F in the form

$$\begin{aligned} \Gamma^{(a)}(F) &= \alpha_a G(\beta_a F) \\ p_{\mathrm{nl}}^{(a)}(F) &= \alpha_a^3 (\beta_a F)^3 M(\beta_a F) \end{aligned} \tag{1}$$

where $G(\mathcal{F})$ and $M(\mathcal{F})$ are the scaling functions or "master curves," and α_a and β_a are two scaling parameters specific to each species a =He,Ne,Ar,Kr,Xe. While the exact properties of the scaling functions are not known analytically, we have approximated them with the parameterizations given below. For the scaled ionization rate G, we have

$$\begin{aligned} G(\mathcal{F}) = \\ \exp[&0.1692048194155632 - 0.810669873391612/\mathcal{F} \\ &+56.391127621143774\mathcal{F} - 823.1689378085457\mathcal{F}^2 \\ &+4152.098445656342\mathcal{F}^3 - 7390.473021873485\mathcal{F}^4 \\ &-0.7555077122737133\log\mathcal{F}] \end{aligned} \tag{2}$$

where the first two and the last term are motivated by the functional form of tunneling ionization rates, and the remaining higher-order terms adjust the functional shape.

For the nonlinear dipole moment, the following

$$\begin{aligned} M(\mathcal{F}) = \\ \exp[&5.049542998716102 + 63.07083179334633\mathcal{F}^2 \\ &+50607.81357765684\mathcal{F}^4 - 6632204.58068692\mathcal{F}^6 \\ &-1019206807.5646534\mathcal{F}^8 + 184485603638.703\mathcal{F}^{10} \\ &-7509132994894.033\mathcal{F}^{12}] \end{aligned} \tag{3}$$

is a representation for the scaled nonlinear index M. The powerful application of these relations is that each species of a noble gas is entirely characterized by only two scaling parameters α_a and β_a. Our subsequent work utilizing these results demonstrated that the universality approach provides a powerful new means of characterization of the nonlinear response and can significantly improve utilization of the measured data (P7).

We have elucidated the physical origin of the universality by using a metastable state analysis of the light-atom interaction in combination with a scaling analysis (Fig. 2).

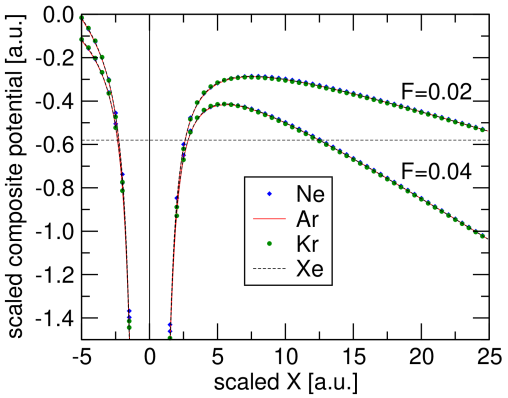

Figure 2: Scaled total composite potentials versus scaled coordinate X for the four noble gas species in the vicinity of the saddle point of the potential. For any value of the external field F, all potential curves of different atomic species coincide after suitable scaling. It is the identical functional shape of the total potential that is responsible for the universal behavior of the optical response.

Our results are extremely intriguing, and invite a conjecture that according to the symmetry of the electronic wave function (or orbital) which contributes most to the optical response, all species fall into different "universality classes." This notion explains a slight deviation in the observed bahavior of helium as compared to the other noble gases (see Fig.1) as consequence of the different symmetry of the higher occupied orbital. Indeed, helium electrons tunnel from the s-like

orbital, while in other gases the active electrons reside in p-like orbitals. It is why one can expect that their scaling functions may be slightly different (one still expects similar functional shapes).

We were able to utilize or numerical results not only to establish accurate representations of the underlying scaling functions M and G (see above), but we have also found the specific parameters corresponding to different noble-gas species. This information provides a convenient way to represent both the nonlinear polarization and also the ionization rate for applications in nonlinear optics.

1.1.2 Stark resonances as a complete basis for open quantum systems

Open and non-Hermitian systems are often characterized by sets of basis functions that form continua, for example in the energy-space. Oftentimes, such continuum-bases can be further degenerate and possibly infinitely degenerate. Obviously, it is practically very hard to work with such bases, and researches have been developing various approaches that aim to replace the continuum of eigenstates with a discrete set of so called quasi-normal states. In the context of the quantum theory, the relevant states can be the so-called Stark resonances when they are induced by the action of an external field.

Intuitively speaking, Stark resonances and the normal Hamiltonian eigenfunctions are solutions to the same (partial-) differential equation, but they are subject to different boundary conditions at infinity. While the standard wave function must be normalizable at least to a delta-function (say in energy), the resonance solutions are required to behave as strictly outgoing (or incoming) waves at infinity. In some cases, an infinite number of resonances exist, and they can be made orthogonal in certain sense. As such, it is a tempting question if it is possible to solve a given problem not with the help of normal Hamiltonian eigenfunction but with the help of the easier to handle discrete (albeit infinite) set of resonance states. In other words, one can ask if the system of resonance states is *complete*, and can serve as a basis.

We have investigated the completeness of the Stark resonant states in a system with a square-well potential and a homogeneous external field (P5). This effort represent a significant generalization of our previous results. Our conclusion is that when the external force pulls the particle to the outside of the system, the resonant-state expansions converge point-wise inside of the potential well as well as on its classically forbidden side. Interestingly, we have found that the existence of convergence is independent of the depth of the potential well. This means, surprisingly, that no matter how shallow the potential might be, there always exists a convergent resonant-state expansion.

We have also derived formulas that show how the rate of convergence depends on the smoothness of the function being expanded. These formulas indicate that the rate of convergence is also independent of the depth of the well, but the absolute size of the terms grows inversely proportional to the potential depth. Thus, for any given target accuracy, a smaller potential depth means that more terms have to be included in the expansion series.

Taking into account the similar nature of the convergence results for the Dirac delta potential studied by us previously and for the potential shapes treated in this work, we have conjectured a similar result for a general potential of compact support. Such a potential can be approximated by a finite set of conjoined square wells, and we expect that our approach can be generalized to this setting using a transfer-matrix technique. In the limit when the set of conjoined square wells approach the smooth potential, there will inevitably be square wells that are arbitrarily shallow but we expect, based on the result derived in this paper, that this will not destroy the convergence. In

fact, this same result led us to conjecture point-wise convergence even for non-compact potentials.

All in all, the results of this works indicate that the intuitive “wishful thinking” that a discrete set of resonance states could be effectively used to by-pass difficulties presented by the continuum nature of the energy spectrum (in systems which are open or lossy) does in fact have a certain justification. Related to this, other results discussed in this report also showed the advantage of the non-Hermitian approach, and we developed practical ways to combine discrete resonant and continuous state-expansion for time-dependent wave functions (P8).

1.1.3 Computational boundary conditions for open systems

In the numerical modeling of unstable and open systems one naturally encounters the issue of the computational domain which must be finite for practical reasons. Numerical solutions face the well-known boundary problem; one needs to terminate the computational volume in a way that mimics infinite space or coupling to the exterior of the system. Because this often requires a large computational domain and fine discretizations, the treatment of the boundaries can add significant cost to the numerical solution.

Such was a motivation for a method we have developed for transparent, energy-dependent boundary conditions for open, non-Hermitian systems. We have illustrated the approach on an example of Stark resonances in a single-particle quantum system (P11). In such a setting, the approach provides an alternative to the commonly applied external complex scaling, resulting in significant computational savings and ability to treat problems at a larger scale. The method is applicable whenever an asymptotic solutions can be characterized at large distances from the origin (and it applies not only to quantum systems but also in optics, for so-called quasi-normal modes in optical cavities and/or in leaky waveguides). Its main benefit consists in a drastic reduction of the dimensionality in the underlying eigenvalue problem.

Besides the application to quantum mechanics, the method can be used in other contexts such as in systems involving unstable optical cavities and lossy waveguides. In fact this is the direction in which further applications are now pursued by J. Heinz, the student responsible for this contribution to our project.

The motivation for and the goal of the new method is illustrated in the following Fig. 3. It shows a schematics with typical features of wave functions in open systems. Here the extended oscillatory portions of the wave function represent the particle escaping towards infinity. This must be accurately captured whenever properties of such unstable states are to be calculated with any accuracy. This is obviously very expensive, and in fact often prohibitively expensive. Instead, our methods allows one to completely eliminate the need to represent the outgoing parts of the systems on a numerical grid. We achieve this by imposing energy-dependent boundary condition which reflect the analytic properties of the exact solution in the asymptotic region far from the origin.

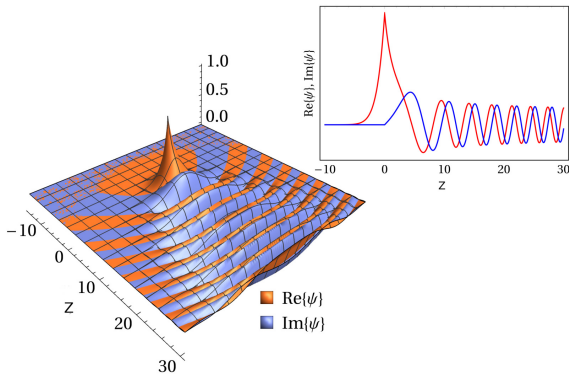

Figure 3: Illustration of the ground-state resonance in a hydrogen-like system in a very strong field. The goal of the method is to completely eliminate the need to discretize the oscillatory tails of such wave functions. Optimally, the computational domain could be restricted to the immediate vicinity of the origin where the solution is also easier to discretize.

An important capability of the method is that the outer solution which is encapsulated by the suitable boundary condition can also exactly include the long-range Coulomb potential. For example, the following was shown to represent a boundary condition in the parabolic system of coordinates (u is the parabolic direction along which the ionized electron escapes) in a singly-charged Coulomb potential combined with a homogeneous external field of strength F

$$U(u) = U(u_{\rm B}) \cdot \frac{{\rm Ci}^{+}\big[-(2F)^{1/3}(\quad u/2 + W/F)\big]}{{\rm Ci}^{+}\big[-(2F)^{1/3}(u_{\rm B}/2 + W/F)\big]} \cdot \frac{G(u\quad, \beta_u)}{G(u_B, \beta_u)} \,. \tag{4}$$

where

$$G(u) = 1 - \frac{2i\beta_u}{\sqrt{Fu}} - \frac{2\beta_u^2}{Fu} - \frac{2i(F/4 - W\beta_u - 2\beta_u^3)}{(Fu)^{3/2}} + O((Fu)^2) \quad , \tag{5}$$

and W stands for the estimated complex-valued energy of the though-after meta-stable electronic state. With this boundary condition valid in the vicinity of the inner-domain boundary set at u_B, the inner-domain eigenvalue problem is solved using any standard method, while keeping the guess of W fixed. Subsequently the resulting eigenvalue is used to update the boundary condition, and the process repeats until the iterations achieve a steady solution. The convergence turns out be be very fast, and despite the fact that the original linear eigenvalue problem has been replaced by a non-linear problem, the size of the latter is so much smaller that the overall computational gain is enormous. The accuracy of the method is very good as illustrated in Fig. 4 where we show examples of imaginary part of the Stark resonance energy for Hydrogen exposed to different fields.

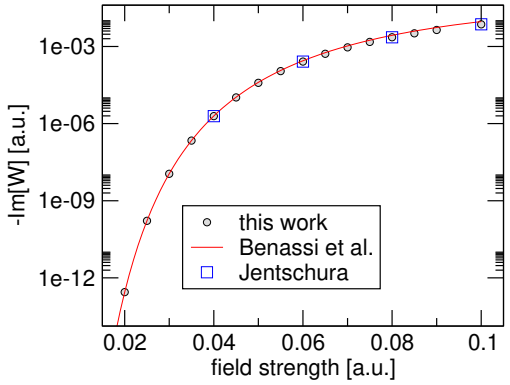

Figure 4: Demonstration of the accuracy: Imaginary part of the ground-state Stark resonance in atomic hydrogen. Circle symbols represent results of the present work, compared to the weak-field asymptotic formula (line) by Benassi et al. [1], and calculations by Jentschura [2]. Note that the the slight difference between the asymptotic formula and our results reflects the loss of accuracy of the former when the field is strong. Our results agree accurately with those from [2] even in strong fields.

This new method became an enabling capability which allowed us to perform necessary calculations in order to create a MESA-based model for the molecular oxygen, a task of significant computational complexity described elsewhere in this report (P9).

1.1.4 Quantum-tunneling dynamics

The tunnel effect [3, 4] has captured the imagination of physicists from the early days of quantum mechanics. One question in particular attracted a lot of attention; namely how long is the time a quantum particle spends inside a potential barrier (see e.g. [5, 6, 7]). This was studied numerous times [8] in various contexts [9] including recent attosecond angular streaking experiments [10, 11]. The physics community has not yet agreed on the answer. On the contrary, development of ultra-precise techniques in the strong-field physics [10, 12] reignited the debate as experiments produced often contradictory results.

Inspired by the ongoing debate, we presented a theoretical study of an exactly solvable model that allows one to accurately characterize the time-dependent wave function of a tunneling particle (P8). Our approach makes it possible to study the dynamics in the regime of a nearly opaque, spatially very long barrier which is difficult to address by other methods (e.g. by solving the time-dependent Schrödinger equation numerically, discretized on a grid). The chosen regime also greatly emphasizes the quantum nature of the effect, by making the deviations from the classical behavior much more pronounced.

We have studied two distinct cases, namely tunneling from a discrete-energy state and tunneling from a continuum, or a band of energies. While the first case mimics an electron escaping from an atom, the second is relevant for electron emission from metallic nano-tips. Different regimes can be obtained as limiting cases of the system sketched in Fig. 5

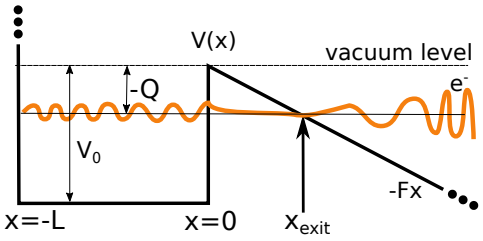

Figure 5: Potential function for a 1D model of a metal nano-tip. For the initial condition given by a zero-field stationary state with energy of $-|Q|$, we aim to calculate the time-dependent wave function of the tunneling particle for locations beyond the classical tunnel exit at x_{exit}. Through the variation of the width and depth of the potential well, different limiting cases of this exactly solvable system can model atoms and/or metal structures.

The technique developed in this work is a rare example of a combination of the resonant-state expansion combined with the expansion in exact quasi-continuum eigen-energy states. We derive *an exact expression for the wave function* $\psi(x,t)$, by deforming the integration contour from one which follows the real axis to one for which the difficult to calculate part of the integral can be obtained from the Stark-resonance poles.

The formally exact (but practically next-to-impossible to calculate) solution can be expressed as an integral along the real axis representing the continuous spectrum of the system. Instead, we choose an integration contour $C=\{z\in\mathbb{C};\,\text{Im}\{z\}=-s\}$ that parallels the real axis in the lower complex half-plane. Utilizing the residue theorem, the expression for the outside wave function

can be written like so

$$\psi(x,t) = -2\pi \sum_p e^{-itW_p} \frac{Ci^+(\alpha(x+W_p/F))}{ND^{+\prime}(W_p)} A(W_p) + \int_C \frac{ie^{-itz}}{N} \left[\frac{Ci^-(\alpha x + \frac{\alpha z}{F})}{D^-(z)} - \frac{Ci^+(\alpha x + \frac{\alpha z}{F})}{ND^+(z)} \right] A(z) dz \tag{6}$$

Here the set of poles W_p (i.e. Stark Resonances) that were crossed by deformation of the contour is finite; it depends on the choice of the parameter s. The discrete sum above is a resonant-state expansion, and its purpose here is to replace the part of the integral that is most difficult to evaluate with the standard Hermitian expansion into Hamiltonian eigenstates of continuum energy. Quantity $A(z)$ characterizes the initial condition by giving the probability amplitude for the energy z. Functions $Ci^{\pm}(x) = Bi(x) \pm iAi(x)$ are combinations of Airy functions, and $D^{\pm}(W) = \pi(Ci^{\pm\prime}(\alpha W/F) - k_W/\alpha \tan(k_W L) Ci^{\pm}(\alpha W/F))/2$ with $\alpha = -(2F)^{1/3}$.

The above is an exact solution to a time dependent wave function of the tunneling particle. As long as the energy-representation of the initial state $A(z)$ can be precisely evaluated this expression is easier to evaluate than it may seem at a first glance. We have utilized this to obtain numerically exact solutions for which some examples are shown next.

In the following, results are shown for a particle suddenly exposed to weak field of $F = 1/100$, and we ask if it is possible to assign a well-defined "classical exit" from the classically forbidden region, and what, if any, temporal delay is associated with the emerging particle. These are precisely the questions debated in the literature, and one reasons they so far proved difficult to resolve is that approximations are necessary in the modeling and interpretation of experiments. Ours are exact results, with no room for interpretation ambiguities...

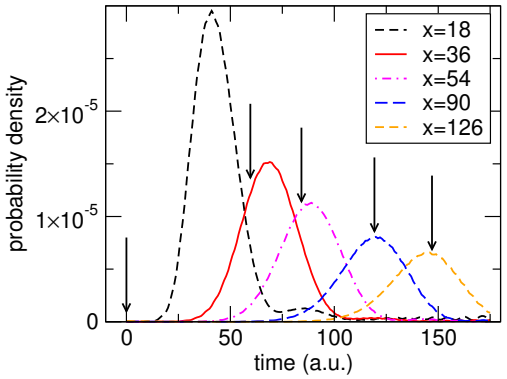

Figure 6: Tunneling particle probability density versus time for different observation locations x. Arrows mark the expected time of arrival for a particle that obeys the simple-man's scenario, which says that that it appears at the classical exit *instantaneously* and with zero initial velocity. Here one can see a pronounced delay, especially for observations closer to the origin. In contrast, when observed very far from the origin, the particle arrives *earlier* than predicted by the simple man's picture.

Perhaps a more intuitive picture of this dynamics is offered by a spatio-temporal map of the particles probability density. This is shown in Fig. 7, where one can appreciate that the process remains very much quantum in nature. Our results show that in one dimension and for a weak external field the tunneling dynamics exhibits a pronounced delay between the sudden switch-on of the field and the time when the particle can be detected at the point of the classical exit from the potential barrier. Moreover, the so-called simple man's scenario of quantum tunneling also does not apply because the particle has a significant velocity when it appears at the classical exit point. *So in this exactly solvable system, one can safely say that the tunneling time is not instantaneous*, in direct contradiction to a number of predictions based on experiments while in agreement with a number of other reports in the literature. However, our results do not support the idea of a well-defined tunneling time either. There are at least two reasons for this. First, it is obvious from the figure below that at the point of classical exit, the temporal distribution of

the probability density "pulse" is actually broader than the apparent tunnel time as defined by the time of arrival of the peak. In other words, the tunneling time is a stochastic quantity that perhaps could be better described by a probability distribution. Second, we have seen that a well-defined moving wave-packet forms actually *before* the particle reaches the classically allowed region. This makes the very notion of the tunnel exit rather ill-defined. By extension the utility of the tunneling time itself is limited at best. However, the time-dependent wave function exhibits a well-defined although fuzzy trajectory, and in this sense the behavior in our illustrations resembles the so-called Wigner scenario.

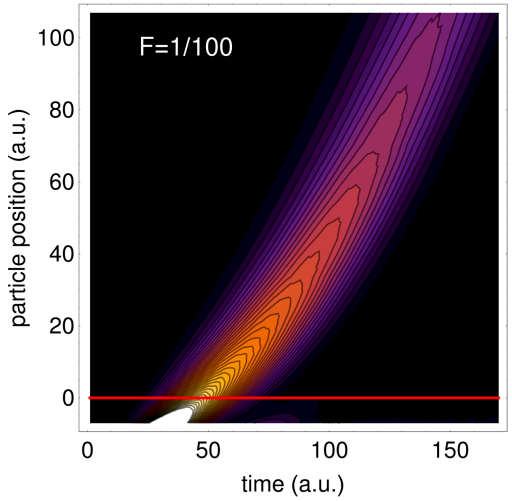

Figure 7: Probability density for the tunneling particle versus time and observation location. The red horizontal line indicates the location of the tunnel exit for the given external field strength. Thus, the area above the line is classically allowed, while the particle is classically forbidden in the region below the line. Obviously, a wave packet headed outwards appears to be formed well before the classical exit point. Moreover, the classically allowed region (above the red line) is only entered after a significant delay. While one could assign a trajectory to the peak-probability loci, the quantum nature of the process is reflected in the strong dispersion (i.e. spreading of the particle's wave packet).

To conclude this section, we would like to point out that the fact that a simple model was utilized for this study still leaves some room for the theory which says that the quantum tunneling happens instantaneously *in the three-dimensional systems*. However, ours is *an exact* solution which shows beyond any doubt that this instantaneous dynamics does not occur in general. In fact, our later work in this project (S1) has shown that even exact time-dependent solutions in three dimensional system show precisely the same qualitative picture revealed by this work.

1.1.5 Exact continuum eigenstates of the Stark-Coulomb Hamiltonian

In calculating the time evolution of a quantum state, the most fundamental approach is to expand the wave function in terms of the eigenstates of the Hamiltonian. However, calculating the eigenstates of the system and *using them as a basis* for the space of quantum states is particularly challenging when the Hamiltonian has a continuous spectrum. For this reason, in most practical situations one resorts to approximations, for example by expanding solutions into approximate, "discretized-continuum" basis.

An important example of a system with a continuous spectrum is the Stark-Coulomb Hamiltonian [13], i.e. the problem of a particle subject to a constant external electric field and a central Coulomb force. The Stark-Coulomb Hamiltonian is important for a number of applications. Recently, experiments on atomic hydrogen [14] exposed to strong electric fields provide a vital testing ground for theory and simulations [10, 12, 15, 16, 14, 17]. Moreover, in ionization of atoms and molecules [18], electrons liberated from the neutral systems experience the Stark-Coulomb potential at larger distances from the nucleus [19, 20, 21]. This composite potential affects the

properties of the electronic wave functions contributing to strong-field ionization [22, 23, 24, 25], and high-harmonic generation. Thus, the numerically exact wave functions of such a problem can be of great practical use. Obtaining such exact solutions was the goal of the work described next (S1).

We would like to note that the problem solved next is not in fact non-Hermitian. However, it becomes obvious in the course of the solution that in order to construct the sought after solutions, it is in fact necessary to understand the details of the underlying non-Hermitian structure embodied by the discrete but infinite set of non-Hermitian quantum states realized in the form of Stark resonances. In other words, the insight that non-Hermitian methods afford in this problem is truly indispensable.

1.1.6 Continuum-energy Stark-Coulomb basis

Problem formulation

We have found all exact solutions, and developed an approximation-free algorithm to evaluate them, for the following Hamiltonian, here written in the frame of reference realized by the parabolic coordinate system (u, v, ϕ):

$$H\Psi(u,v,\phi) = W\Psi(u,v,\phi) = -\frac{2}{u+v}\left[\frac{\partial}{\partial u}u\frac{\partial\Psi}{\partial u}+\frac{\partial}{\partial v}v\frac{\partial\Psi}{\partial v}\right]-\frac{1}{2uv}\frac{\partial^2\Psi}{\partial\phi^2}-\frac{2\Psi}{u+v}-F\frac{u-v}{2}\Psi$$

where F is the strength of the homogeneous external field. Without any loss of generality we will assume that this quantity is positive. W stands for the energy eigenvalue, which can take on any real value. Our goal is the capability to expand an arbitrary time-dependent wave-function in the eigenenergy basis of this Hamiltonian as

$$\Psi(t) = \sum_q \int dW A_q(W) e^{-iWt}\Psi_{qW} \ , \tag{7}$$

where $A_q(W)$ is the wave function in the energy representation, and it can be understood as the overlap integral between the given quantum state (at time $t = 0$) and the corresponding eigenstate. The discrete index q stands for the pair made of the magnetic quantum number m and and integer n which counts the number of zeros the wave function has along the v-coordinate axis.

It is crucial that the eigenstates are constructed and normalized such that the resolution of unity in energy holds, namely

$$\langle\Psi_{nW}|\Psi_{mE}\rangle = 2\pi\int\frac{u+v}{4}\Psi_{nW}(u,v)\Psi_{mE}(u,v)dvdu = \delta_{nm}\delta(W-E) \ .$$

It is indeed this orthogonality requirement which presents the biggest challenge. It is relatively easy to obtain an un-normalized eigen wave function for the given problem, but without normalization such states are of little use. However, achieving accurate normalization to a Dirac delta function in energy is highly nontrivial. We have solved this problem by developing a version of analytic continuation of the solution such that we can start at the origin and extend an arbitrarily accurate solution to very large distances. The accurate relation between the wave function behavior around the origin and in the asymptotic region is key for achieving proper normalization.

Eigenstates for the energy continuum

It is important to formulate the solution in a way that completely eliminates any need to solve

numerically the underlying differential equation(s). What we aimed for is essentially yet another special function, and not a numerical solution of a PDE. Our exact derivation resulted in the following formulas for all eigenstates (for simplicity, here we only list results for $m = 0$)

$$\Psi_{nW}(u,v) = v_{n0}(W)M(W, z_v(n,W,F), F|v) \times u_{n0}(W)M(W, 1 - z_v(n,W,F), -F|u) \tag{8}$$

where the function M is a series specified by the coefficients obtained from the recursion

$$\begin{aligned}
m_0 &= f,\\
m_1 &= p,\\
m_2 &= \frac{1}{2a}\left(\frac{Fa^2m_0}{4} - \frac{aWm_0}{2} - zs_0 - m_1\right),\\
m_3 &= \frac{1}{6a}\left(\frac{Fam_0}{2} - \frac{Wm_0}{2} + \frac{Fa^2m_1}{4} - \frac{aWm_1}{2} - zm_1 - 4m_2\right),\\
m_k &= \frac{1}{k(k-1)a}\left(\frac{Fm_{k-4}}{4} + \frac{Fam_{k-3}}{2} - \frac{Wm_{k-3}}{2} + \frac{Fa^2m_{k-2}}{4} - \frac{aWm_{k-2}}{2} - zm_{k-2} - (k-1)^2m_{k-1}\right)
\end{aligned} \tag{9}$$

in which parameters f, p, a represent the value, derivative, and the central point for the series. The separation constant $z_v(n,W,F)$ is fixed by the requirement that the v-dependent part of the function vanishes at infinity, and $v_{n0}(W)$ is the corresponding normalization factor.

The most nontrivial quantity is u_{n0} which is obtained from the solution of the linear system of two equations in which u_i are distinct but otherwise arbitrary points on the u-axis:

$$u_{n0}(W,F)M_a(W, 1 - z_v, -F|u_i) = \frac{1}{2N_U}Ci^+\left[\alpha\left(\frac{u_i}{2} + \frac{W}{F}\right)\right]H(u_i)e^{i\delta_n(W,F)} + c.c. \quad i = 1,2 \tag{10}$$

The "envelope function" H can be specified by an approximation-free asymptotic expression

$$H(u) \sim \frac{1}{u^{1/2}} - \frac{2iz_u}{F^{1/2}u} - \frac{2z_u^2}{Fu^{3/2}} + \frac{i(8z_u^3 + 4Wz_u - F)}{6F^{3/2}u^2}\ldots \tag{11}$$

where more terms can be calculated with some effort.

The above recursion is used in an analytic continuation which is initiated at the origin and proceeds to the region where the the accuracy of the above representation of function H is sufficient (e.g. 10^{-12}). Similar, albeit a bit more complicated formulas can be given for the states with non-zero magnetic quantum number m.

The algorithm which we designed deliberately avoids any numerical solutions of differential equations, and it represents essentially a formula, albeit a more complex formula. In effect, the evaluation of the exact Stark-Coulomb eigenstates is about as complex numerically as an evaluation of a special function. The algorithm is also highly accurate (in fact it can be executed with an arbitrary accuracy), and we demonstrate its accuracy in Fig. 8. It shows the most sensitive quantity in the whole evaluation, i.e. the amplitude $u_{0n}(W)$ which holds the signature of the Stark resonance. It comes in the form of an extremely sharp peak, which is best appreciated on the logarithmic scale used in the figure.

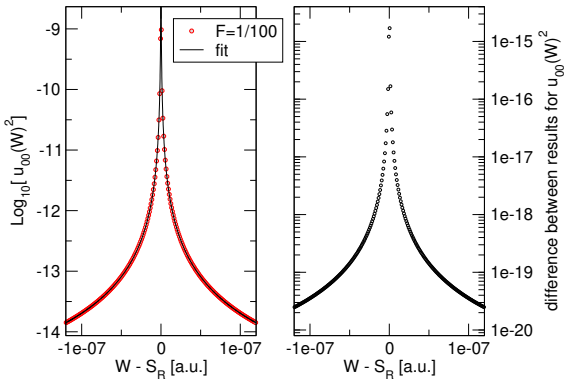

Figure 8: Left: Behavior of $u_{00}^2(W)$ in the vicinity of the Stark resonance energy $S_R = -0.500225560455....$ This data allows to estimate the location of S_R with an accuracy of 10^{-12}. Right: Demonstration of the robustness w.r.t. choice of the join-points $u_{1,2}$. The plot shows the difference between results obtained with $u_1 = 2900, u_2 = 2910$ and with $u_1 = 3900, u_2 = 3910$ (for Eqn. 10).

This figure shows not only that the solution does not depend on the choice of the "hyper-parameters" (i.e. quantities that control the evaluation of the function, but which do not carry physical meaning in the given problem). It also demonstrates the excellent accuracy. Here, in the right-hand-side panel, we can see that the relative accuracy of the most sensitive quantity in the whole evaluation can easily reach a part in million, while the absolute accuracy is of the order of 10^{-12}.

An important feature of our method is that there are two complementary representation of the wave function; one is a series and the other expressed in terms of a "carrier-function" and its "envelope" H. The latter can be utilized to obtain solutions and also their quasi-classical representation in extremely large distances from the origin (something that would be utterly out of reach of other numerical methods). So our method also provides a useful tool to address questions concerning the tunneling time as discussed earlier.

1.1.7 Exact time-dependent description of a tunneling electron

As a first demonstration of the application of our algorithms, we have studied the time-dependent aspects of the electron tunneling from a hydrogen atom. While this study generalized our previous work, *this represents the first exact treatment of the time-dependent wave function in a realistic three-dimensional model*. As such it is of great value, in particular as a contribution to the still ongoing debate about the nature of the "tunneling time."

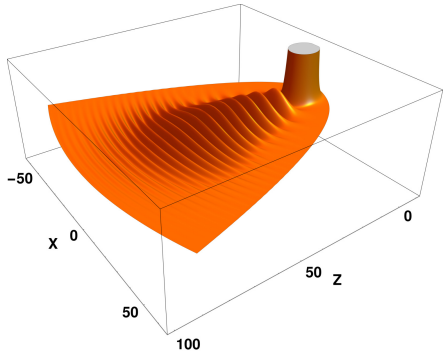

Figure 9: Wave function snapshot taken at time $t = 60$a.u. The real part of the component $n = 0$ is shown here with the vertical plot range of ± 0.001. The cut-off part in the center (the "stump") is the (slightly deformed by the field) wave function remaining in the metastable ground state which will "survive" for $\sim 10^{10}$ atomic units of time. In contrast, the waveform will propagate away from the atom very quickly, and thus contributes to the non-adiabatic ionization.

Figure 9 depicts a snapshot of the wave function of the electron which tunnels from the hydrogen atom, initially in its ground state, after a sudden exposure to a constant electric field. Shown is the $n = 0$ component, in which two parts can be identified. The first the portion of the wave

function still remaining in the metastable state similar to a deformed (by the field) ground-state. This is visible in the figure as the cut-off "stump" because a thousand times larger vertical scale would be needed to depict this part of the wave function in its entirety. The escaping wave packet represents the electron emitted in a non-adiabatic regime from the atom. When one observes this as a function of time, it becomes obvious that the emergence of the tunneling particle is *delayed* with respect to the moment when the external field was turned on. So this tunneling regime is manifestly non-instantaneous.

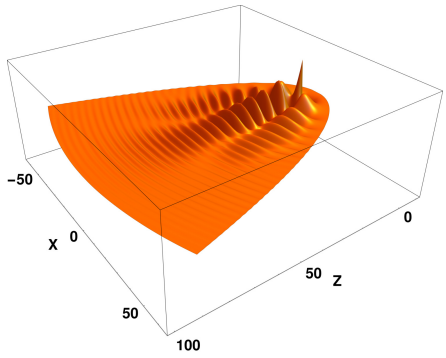

Figure 10: Wave function snapshot taken at $t = 60$a.u. The real part of the component $n = 1$ is shown here with the vertical plot range of ± 0.001. The spatial structure indicates that one can't assign a single classical trajectory to this tunneling particle. Moreover, no single "exit point" (or point of emergence) can be assigned to this wave function.

Figure 10 shows the $n = 1$ component of the wave function under the same conditions and at the same time. Despite the fact that a major portion of the wave function is in the classically allowed region, even its main features (such as local maxima) could not be described in terms of a single classical trajectory.

Thus, our results show beyond any doubt that the tunneling dynamics continues to be quantum in nature even beyond the emergence of the particle from the classically forbidden region. Should one insists on assigning a tunneling time to this process, it would be decisively not instantaneous. Moreover, our exact results clearly do not support the idea of zero initial velocity. As such we can conclude that the so-called simple man's scenario of quantum tunneling can not be considered as more than a very approximate description. Instead, proper quantum description should be preferred also in the outer regions, and this should connected to the classical description of a particle ensemble characterized by a probability distribution for initial times, and initial velocities. Our representation of the Stark-Hydrogen solutions represent an ideal tool for such an application, and we trust they will contribute decisively to the resolution of the tunneling-time problem.

1.1.8 Impact and future applications

The results described in this section are rather unique from a couple of different standpoints. First, it is important to note that there are extremely few examples where a *system with a continuum spectrum* can be efficiently treated with the state-expansion using Hamiltonian eigenstates. Textbooks typically do not go beyond a formal but practically very limited expansion formulas, In applications, energetic continua are approximated as dense but still discrete sets. In fact, our result is the first exactly solvable case for a three-dimensional realistic system where the eigenstates are formulated in a way that permits useful calculations without resorting to finite domains and quasi-discrete numerical energy spectra. As such, our results are of importance for the future design of numerical algorithms, and they open a door to working with energy-representations of wave functions. The fact that Stark-Hydrogen Hamiltonian appears in the form of the asymptotic behavior in all atomic and molecular species that ionize sequentially make our result broadly applicable.

Beyond computational physics, already the results laid out here present the necessary tool to address certain fundamental questions concerning the light-matter interactions in the strong-field regime. As an example one can consider the question of the "instantaneous electronic response." It is assumed universally that for all practical purposes in nonlinear optic, the electronic part of the optical response if instantaneous. In other words, it does not depend on the history of the systems, and the electrons respond so fast that the time they need to adjust to the change inthe external force vanishes. This is obviously merely an approximation, simply justified by the gap between the optical and atomic time-scales. Nevertheless, very little is known about how fast in fact the electronic response is. Beyond a lone recent experiment [26] and order of magnitude estimates given in textbooks, nothing quantitative is known about what is truly fundamental question. Now with the Stark-Coulomb exact states formulated in a way that admits practical calculations, we can, for the first time, address these questions by "simply" expanding time-dependent solutions or transients in the wave functions after fast changes in the optical fields. Such investigations are underway.

1.1.9 Connecting quantum and classical description in quantum tunneling

The particular work described next (S3) was inspired by the long-standing interest in the conceptual questions related to quantum tunneling, as well as by the current debate in the literature which was re-ignited by modern experiments. Many studies in the strong-field area require that a connection is established between the quantum-level dynamics in atoms or molecules and the classical description of emitted electrons, and this serves as a motivation for this work.

Drawing on our previous work described elsewhere in this report, our goal was to present a model framework to explore the dynamics of quantum tunneling in detail and from several standpoints. The work is based on a an exactly solvable model constructed such that numerical, exact, and approximate solutions can be all explored, compared, and used to elucidate the time-dependent wave function of a tunneling particle with emphasis on questions concerning the possibility of classical or quasi-classical description *after* tunneling from the atom.

Motivated by dissemination of our result widely, we decided to make all components of this study, and in particular the mathematical and computation tools required, accessible to students with some help from their teachers, and present the material in the American Journal of Physics. We selected the material which can serve as a basis for a supervised case-study, perhaps as a part of an advanced class on quantum mechanics or computational physics, offering students an opportunity to practice several important techniques and do this while learning about a problem that is still debated in the literature.

We approach the problem with a spectrum of techniques developed in this project, and chose some of them which all aspiring practitioners of quantum theory need to master: We first guide the reader through a numerical solution. Then we introduce an exact solution for the time-dependent wave function of the escaping particle. Importantly, this also provided a very rare example of a practically usable continuum state-expansion. Finally, we explored the notion of Wigner trajectory and ask if the escaping electron can be described in classical terms. We trust that this "technique sampler" will be of interest for learners and educators alike, and believe that this work will make our results more accessible to a wider audience.

From the physics standpoint, the focus was on the applicability of the Wigner-trajectory description of a particle (electron) escaping form a (model) atom. The notion of the Wigner trajectory is often applied in the context of many modern experiments in which atoms and/or molecules are

exposed to strong optical field, tunneling electrons are subsequently detected, measuring their locations and velocities. From such data, inferences on the dynamics of the quantum-tunneling are made. Obviously, the end-point description of these electrons is purely classical, even if they originate in the process (i.e. tunneling) which is quantum in its nature. So it is necessary to make a connection between the two regimes, and the Wigner trajectory is one of the approaches widely used.

While the emphasis of this work was on its education value (hence the choice of the journal), the central results are very much relevant for the currently debated topics in the strong-field literature. We have shown that the Wigner trajectory, when taken at its face value does not describe the escaping electron very well. This failure is illustrated in Fig. 11 showing the modulus of the wave function of an electron escaping from a model atom after sudden exposure to an external electric field. For this comparison with the exact results we have used the standard definition of the Wigner trajectory which assumes that the trajectory is governed by the energy equal to that of the initial bound state. Obviously, the prediction based on the notion of the Wigner trajectory is rather poor. Note that this prediction is similar to the so-called simple man's scenario which says that the electron appears at the classical exit point instantaneously and with zero initial velocity. This is clearly far from what the exact solution shows, and we must conclude that the description is just too simplified to capture the most important features of escaping wave function.

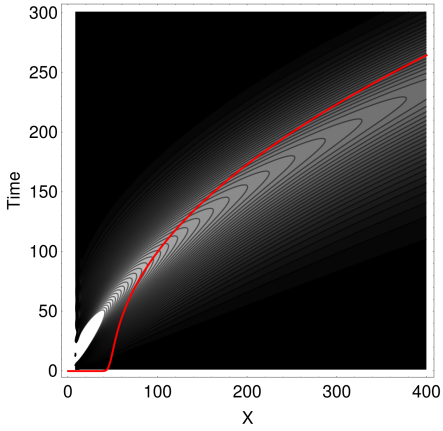

Figure 11: The comparison between the exact numerical solution and the Wigner's trajectory calculated at the energy $W = -1/2$, equal to the energy of the initial state. This trajectory is in fact very close to that of the so-called simple-man's scenario [50] in which the particle emerges from the classical exit point with zero velocity [51].

However, we also asked if it is possible to adjust the selection of the Wigner trajectory so that it would be better suited for at least an approximate description of the tunneled electron. We have come to the conclusion that the concept can be salvaged in some circumstances. This is illustrated in Fig. 12, which shows how the exact solution compares to a modified Wigner trajectory. The modification consisted in choosing the energy for which the trajectory is calculated by the stationary-phase method. This was based on the results form the exact state-expansion approach which showed that the mean energy of the time-dependent solution is in fact much higher that the energy of the initial bound state.

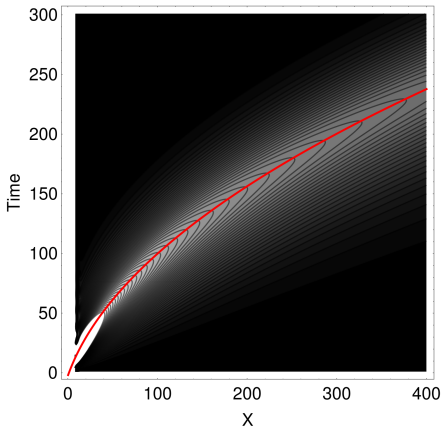

Figure 12: The comparison between the exact numerical solution and the Wigner's trajectory calculated at the energy $W = +0.11$ roughly corresponding to mean-energy of the time-dependent state-expansion solution.

So what we have found is that *when armed with additional knowledge about the actual (mean) energy* one can indeed accurately approximate the evolution of the peak of the probability density with the appropriately chosen Wigner trajectory. In other words, the notion of the Wigner trajectory must be modified by dropping one of its assumption, namely one that says there is a single energy value equal to that of the initial state which should be used to calculate the trajectory.

However, it would be dangerous to jump into a conclusion that a suitable Wigner's trajectory can be found for all similar situations. In fact, when one considers a time-dependent external field which varies more gradually, a highly localized wave packet can still be obtained, but a single suitable Wigner's trajectory can not be easily selected. Specifically, the numerical solution of TDSE will quickly reveal that not a single but perhaps a *bundle of classical trajectories would be more suitable* in a situation with a gradually ramped-up field strength ($F(t) \sim t$).

All in all, our investigations, which are largely based on exact results for simple models and therefore leave little room for doubt, suggest very strongly that in general it is not realistic to hope for an accurate description of the tunneling electron in terms of a single (however chosen) classical trajectory.

1.2 Metallic nano-structures exposed to strong field

Metallic structures interacting with electromagnetic fields exhibit properties similar to those found in atoms and molecules, such as multi-photon and tunnel ionization. We have developed (P12) this similarity beyond the electron emission current, and generalized the well- known Fowler-Nordheim model for electron emission from a nano-scale metallic tip. We have predicted a heretofore unrecognized source of nonlinear optical response from nano-structures exposed to illumination with intense optical pulses. We have also predicted that the harmonic generation by these structures is non-perturbative in the sense that higher harmonic orders can be almost as strong as the lower orders.

1.2.1 Generalization of the Fowler-Nordheim approach

It has been recognized that the behavior of nano-structures exposed to optical pulses exhibits some important similarities to the dynamics of single atoms in an external field [27] such as multiphoton ionization [28] and strong field ionization [29]. However, so far the parallels have been

recognized only for the liberated electrons; Here we discuss our extension of this connection also to the polarization aspect of the optical response.

In atomic and molecular systems there is always a nonlinear polarization response which accompanies the strong-field ionization [30]. In fact, whenever the external field becomes strong enough to cause field-ionization, it also necessarily gives rise to a dipole moment as a result of the deformation of electronic wave functions [31]. As a result, the ionization and the nonlinear polarization of atomic and molecular species exposed to strong electric fields are closely connected [32]. The interplay between the polarization and ionization gives rise to physics driven by both the bound and the freed electrons, governing many phenomena in modern nonlinear optics, including optical filamentation [33] and long-distance localized pulse propagation [34]. It is fair to say that whenever ionization by a strong electric field can be detected, the nonlinear polarization response is already so strong that it must not be neglected. This begs a question if such a connection should be made for nano-structures.

As the first step, we have created a new exactly solvable model. On one side, it can be shown that after additional approximation the so-called Fowler-Nordheim model [35, 36, 37] can be obtained to describe the electron emission from a metal nano-structure under the influence of the external field. However, our approach is non-Hermitian from the get go, and we treat the system as open, and use the meta-stable resonance states as our basis. The comparison with the limit in which the Fowler-Nordheim model is recovered was done as the step in which we demonstrate the viability of the approach.

1.2.2 Nonlinear polarization and high-harmonic radiation from metallic nano-tips

Having successfully reproduced the F-N per-state-current in our non-Hermitian formulation, we can show the strengths of this formalism by calculating the dipole moment and eventually the surface polarization of the nano-structure irradiated by an external field. This gives us an experimentally testable prediction which could not be made using the scattering states utilized by the standard model.

The resulting dipole moment shows a highly non-linear behavior with respect to the external field. The physical reason can be inferred from the fact that the electric field does not penetrate easily beneath the metallic surface, and a strong asymmetry arises when the external field changes its polarity. This alone suggests that a strong second- and higher-order harmonic generation should occur.

However, the important question is about the strength of this nonlinear polarization contribution which is localized in the vicinity of the metal-vacuum interface. We have quantified this is terms of comparison with the counterpart effect in noble gas atoms. The results are illustrated in Fig. 13 where we compare the surface nonlinear dipole density to what it would be for the same density of noble-gas atoms. In other words, noble gases are used here to define the “measurement unit” of the nonlinear optical polarization. The pronounced nonlinearity of these repose curves is evident from the data, as well as the fact the relevant behavior occurs precisely in the region of field strength which represents the typical regimes achieved in ultrafast laser pulses.

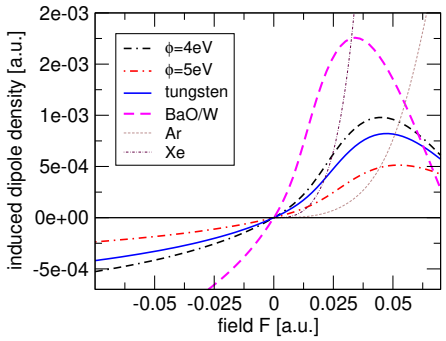

Figure 13: Induced dipole moment density obtained for workfunction values ϕ representing the range typical of metals. For comparison, thin lines represent the response of noble-gas atoms scaled to surface atom-density of tungsten. While the nonlinearity per atom is similar to that of noble gases, it is evident from the peaks in the dipole curves that *higher-order nonlinearity* appears much stronger than in gases.

So these calculation indicate that the surface non-linearity is indeed strong, in fact comparable to that of the most nonlinear noble-gas atoms. Of course, manifestations of the nonlinear dipole density induced on the surface of a metallic nano-structure will obviously depend not only on the material but also on the geometry of the surface and on the parameters of the excitation by optical pulse.

We have considered harmonic generation as one possible effect that could be utilized for the detection of the nonlinear response mechanism put forward in this work. We envisioned a situation in which a large collection of nano-tip structures [38, 39] is irradiated by an optical pulse, giving rise to a coherent array of nonlinear oscillating dipoles. The spectral content of the re-radiated field will reflect the properties of the individual structure, and this is illustrated in the following Fig. 14

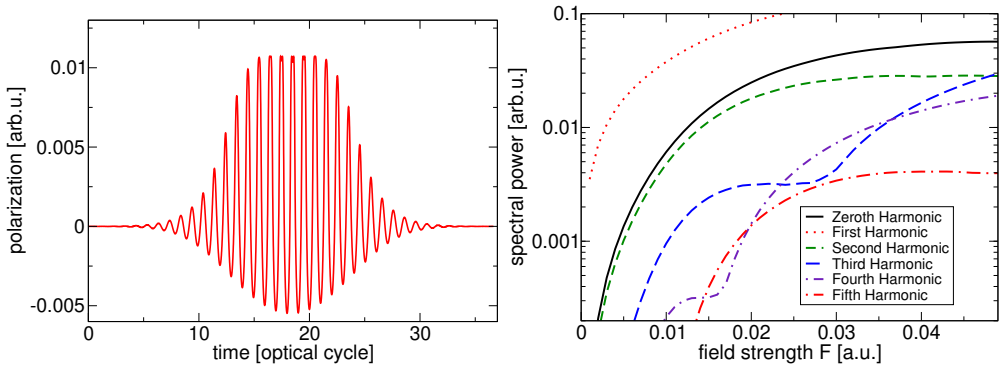

Figure 14: Harmonic generation due to nonlinear polarization on surface of tungsten. Left: A sample of polarization induced by a Gaussian driving pulse with amplitude $F = 0.04$a.u. Asymmetry and saturation of the induced dipole indicates strong higher-order nolinearity. Right: Spectral power integrated over harmonic-frequency bands shows strong contribution of higher harmonics.

Figure 14 illustrates the non-perturbative nature of the nonlinear dipole induced on the surface of tungsten, taken as an example of a material often utilized to manufacture metallic nano-tips. For this illustration, it was assumed that a nano-tip was irradiated by a Gaussian optical pulse, and we calculated the surface polarization response. This is shown in the left panel of the figure.

An interesting signature is a well-developed up-down asymmetry of the polarization pulse, which signifies strong second-harmonic generation as well as an optical rectification signal in the zero-harmonic frequency range. Another feature visible in the polarization is the saturation when the field is strong enough to reach the peak shown in Fig. 13; for very strong fields the response-curve stops increasing, and this manifests as a saturation of the response. However, saturation

does not imply a weaker response. In fact, it signifies that the relative strength of the higher harmonic components increases.

One can also clearly see that different functional shape occurs around the positive and negative peaks, when the former appear blunt while the latter are more pointed. This means that the polarization does not exactly imitate the sinusoidal form of the incident pulse and that the single frequency carried by the incident pulse is now mixed with other harmonics to create the polarization-response pulse.

The panel on the right hand side of Fig.14 illustrates the power integrated in each harmonic frequency band and shows several of these bands as functions of the driving field amplitude.

The important property that reflects the highly nonlinear nature of the response is that several harmonic frequencies exhibit power levels which are quite comparable, being all within a one to two orders of magnitude range when the irradiating field is strong. It can even happen that a higher harmonic becomes stronger than its lower-order counterpart. The non-monotonic increase with the driving field amplitude is another signature that seems universal, although the precise shape depends on the material (i.e. mainly on its work function). All in all, this predicted behavior of higher-harmonics radiated from the nano-structure is rich in signatures which could allow future experiments to distinguish this source from others, such as the classical second-harmonic.

1.3 Extreme nonlinear optics with Metastable Electronic State Method

In this section we concentrate mainly on those works that were done in collaboration with outside experimental groups. As the tools developed in this project enabled much of our contribution, we characterize these works as applications.

1.3.1 Utilizing universality and experiments to calibrate optical nonlinear response

One of the outcomes of this effort was a proposal for the universality of the nonlinear response (P6), including the induced nonlinear dipole and the ionization rate in the strong optical field. We have put to this concept to a test and used it to significantly improve the accuracy of a previously designed MESA-type model for Xenon (P7). Utilizing experimental data from H. Milchberg group which resolved both the nonlinear polarization and ionization in time and space, we applied the theory described elsewhere in this report to calibrate the scaling parameters of the Xenon model. While using a single experiment to adjust the species-specific scaling parameters of the Xenon atom, we have demonstrated an agreement with several independent experiments used as rigorous out-of-sample test. Importantly, the measured and modeled behaviors spanned the intensity range relevant for applications in nonlinear optics at near-infrared and mid-infrared wavelengths. This project not only *verified the concept of universal nonlinear response we have proposed earlier*, but it also showcased the practical utility of the concept. Namely, we were able to take experimental data with significant levels of noise (note that the underlying experiments are truly one of a kind and extremely demanding, so certain amount of experimental noise must not be taken as a signature of inaccurate measurement) and we were still able to make use of it.

Based on a numerical and theoretical study described elsewhere in this report, we have have established that the nonlinear optical response of noble-gas atoms can be described in a unified form [40] given by

$$P_{\mathrm{nl}}^{(a)}(F) = \alpha_a^3 \mathcal{F}^3 M(\mathcal{F}), \quad \Gamma^{(a)}(F) = \alpha_a G(\mathcal{F}), \tag{12}$$

where two scaling parameters α_a and β_a are specific for each atom, the scaled field strength $\mathcal{F} = \beta_a F$, and universal functions $M(\mathcal{F})$ and $G(\mathcal{F})$ represent the nonlinear induced dipole and the ionization rate, respectively. The strength of the above statement can be hardly overstated; it implies that there are only two parameters which are allowed to be adjusted once, and subsequently the theory must capture or describe any other experiment involving nonlinear polarization and ionization in strong field.

An important feature is that while different models of an atom (e.g. realized with different single active electron potentials [19, 41]) may give different values for the response, the functional shape turns out to be quite robust [40]. In other words, while a model may get the scale wrong, the functional shape of the response can still be close to the "master curves" $M(F)$, $G(F)$. This realization invites one to try to find appropriate scaling parameters α_{Xe} and β_{Xe} from a comparison with an experiment, while keeping the the master curves unchanged. In order to express the adjustment as a modification of the original theoretical parameters, we replaced

$$\alpha_{\mathrm{Xe}} \to a\alpha_{\mathrm{Xe}} \quad \beta_{\mathrm{Xe}} \to b\beta_{\mathrm{Xe}} \tag{13}$$

in the formulas specified in Ref. [40]. A large number of simulations of *a single experiment* were executed varying calibration values a, b in a vicinity of unity, arriving at $a = 0.91$, $b = 0.99$, the values that represent the required adjustment of the theoretical α_{Xe}, β_{Xe}. Figure 15 illustrates this calibration process using a single experiment.

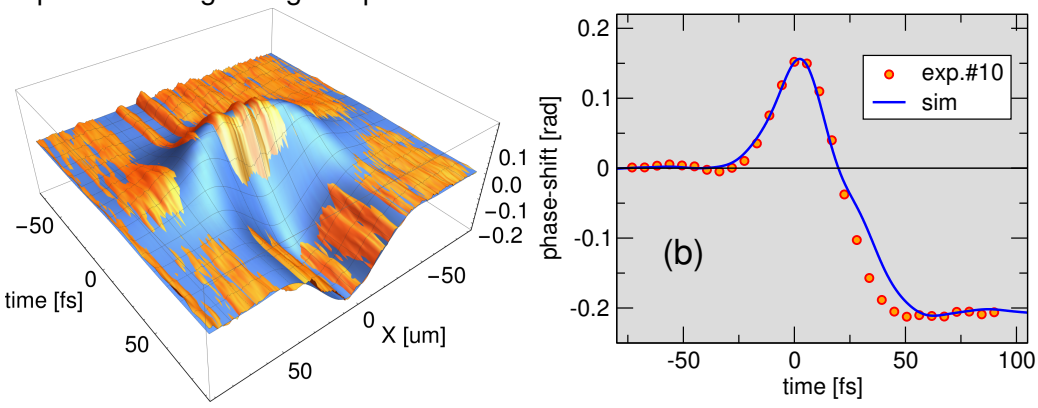

Figure 15: Nonlinear phase shift in a pulse propagating across a Xenon gas jet. a) Blue (simulation) and orange (experiment) surface plots show a typical spatial-temporal phase-shift profile. b) The time-dependent phase shift for a spatial point on the beam axis. Data is for experiment #10, with the peak pump intensity measured in the range 46.5-50.4TW/cm^2. The full line represents the simulation result with the calibrated scaling parameters.

As out-of-sample test, Fig. 16 shows the resulting agreement with the experimental data not used in the calibration. Importantly, a consistent experiment-theory agreement is evident in very different regimes; while on the left we have an example in which the ionization response is relatively strong, the right-hand-side panel shows a case dominated by the Kerr self-focusing nonlinearity.

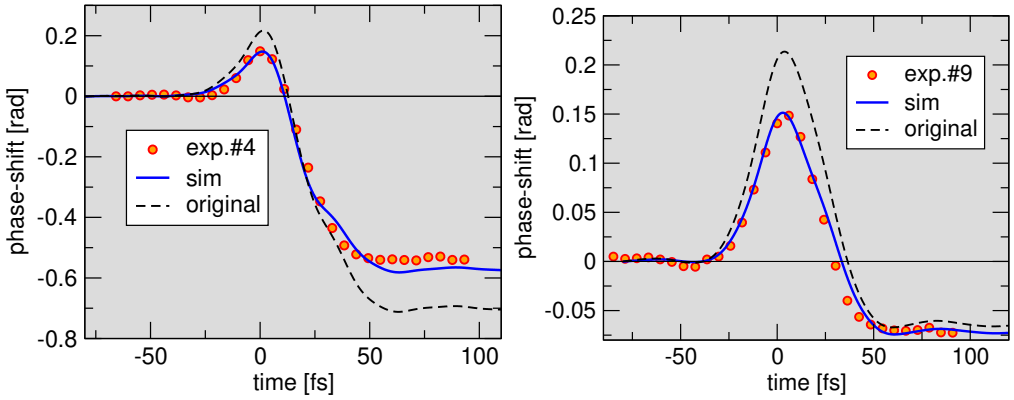

Figure 16: On-axis nonlinear phase shift as function of time. The peak measured intensity were 57-62TW/cm^2 and 35-39TW/cm^2 in (a) and (b), respectively. The full lines represent the the simulation results from the calibrated model, and the dashed lines are from the original model. Positive values are due to self-focusing nonlinearity, while negative values reflect the density of freed electrons.

In summary this particular work provided the first experimentally based evidence supporting the concept of universal behavior in the nonlinear optical response. Moreover, it provided a concept for how the universality can be utilized to extract as much as possible from the experimental data even in situations characterized by significant levels of noise. Moreover, we have also shown that the simulation-aided processing of the experimental data can by-pass its weakest or most difficult step which is a precise determination of the focal intensity (due to the combined effects of propagation and nonlinearity is is far from straightforward to measure the actual peak intensity accurately). In other words, knowing the universal functional shape of the nonlinear response makes it possible to accurately estimate the pulse energy in each of the independent experiments.

1.3.2 Post-Kerr-like optical-response nonlinearity

Despite the debates that occurred in the literature dealing with the nonlinear optics of gaseous media exposed to high-intensity optical pulses, there are still unresolved questions about the nature of the optical response. This is especially true for the regimes in which both the bound- and freed electrons simultaneously contribute tho the light-matter interaction dynamics.

We have designed a study (conceived before the start of this project but finalized here) based on comparative numerical simulations of optical filamentation to shed light onto a long-standing question about the importance of the higher-order nonlinearity. We have shown that while the influence of higher-order effects is small, they do affect the collapsing beam as it propagates through the onset of the optical filament. The higher-order nonlinear interactions may not change how the collapse is eventually arrested, but they influence the filament dynamics by making the increase of the near-collapse intensity steeper.

One important observation we put forward is that the filamentation is not governed by the true Kerr effect, because this strictly third-order nonlinearity only occurs at intensities that are on the lower end of the range typical for optical filamentation. Rather, the filament experiences a nonlinear response that is in fact stronger than that corresponding to the purely third-order. In other words, the experiments that claim to measure the Kerr nonlinear coefficient, i.e. the nonlinear index,

do not in fact probe this elusive value. Instead they produce an effective nonlinear index which depends on the intensity range employed in a given experiment.

A practically important insight from our simulations concerns the question if the filamentation can be modeled with a simple third-order nonlinear Kerr effect. Our result show that one can indeed choose an *effective value of the nonlinear index* for which the properties of the simulated filament become quite close to those seen with the full-nonlinearity model. Crucial from the modeling point of view, the fact that choosing the effective nonlinear index equal to experimental provided acceptable match with the full model is an indication that at least at longer wavelength in the MIR region the MESA-based description of the filamentation should agree with the experiments. It also sheds new light on our previous comparison of the MESA-derived values of the nonlinear index with the experiments; In this hindsight, the gap between the theory and measurement reflected the difference between the true and effective Kerr nonlinearity.

Having shown that the higher-order nonlinearity has a subtle contribution to the filament formation, we have also seen that this contribution can be approximately captured by an effective third-order medium. This is why we suggest that any measured value of the nonlinear index obtained under an assumption of third-order nonlinearity should be considered as effective in the specific range of light intensities over which it was measured. While new schemes to quantify the higher-order nonlinear contributions are being developed [42], also highly accurate measurements of the nonlinear index at very low intensity should provide a way to verify the difference between the truly low-field nonlinear index and the effective nonlinearity for the intensities approaching or beyond the ionization threshold.

1.3.3 Meta-stable electronic states in multi-electron systems: Molecular oxygen

In a push to finalize the collection of MESA-based models needed for the numerical modeling of high-intensity optical pulses propagating in gases and specifically atmosphere, we turned to the last missing piece which was the molecular oxygen (P9). This task was challenging not only because the molecule is inherently a multi-electron system but also because even after the initial multi-particle calculations followed by the transition to an approximated effective single-active electron regime, the computational problem still remains formidable. Not only is the size of the underlying non-Hermitian eigenvalue problem very large, but it must be solved many times in order to obtain the resulting effective optical response of a gas comprised of randomly oriented molecules.

This project required the development of new numerical methods specifically tailored for the open quantum systems — the algorithmic part of this task is described elsewhere in this report in particular in the section dealing with numerical boundary conditions for non-Hermitian eigenvalue calculations (P11). Once the enabling algorithms and tools were available, we presented a computational model for the nonlinear response of the molecular oxygen exposed to strong mid-wavelength and long-wavelength infrared optical fields.

The crucial step was the transition from the many-body quantum calculations (employing the density functional theory) to the effectively single-active electron problem. The former must be solved on a relatively compact domain (see Fig. 17).

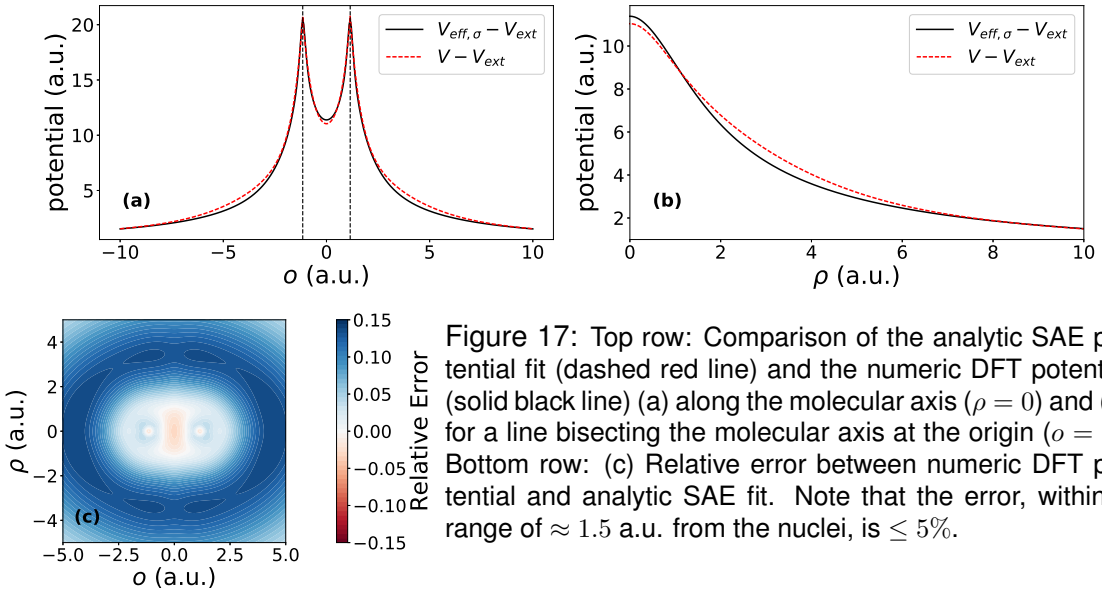

Figure 17: Top row: Comparison of the analytic SAE potential fit (dashed red line) and the numeric DFT potential (solid black line) (a) along the molecular axis ($\rho = 0$) and (b) for a line bisecting the molecular axis at the origin ($o = 0$). Bottom row: (c) Relative error between numeric DFT potential and analytic SAE fit. Note that the error, within a range of ≈ 1.5 a.u. from the nuclei, is $\leq 5\%$.

However, calculations of the meta-stable states are exceedingly sensitive to the properties of the potential in the asymptotic region far from the core of the molecule. That is why it was necessary to "extrapolate" the effective potential experienced by the active electron onto a significantly larger domain. The size of the domain was dictated by the requirement that that potential was asymptotically approaching the long-range Coulomb force field as illustrated in Fig. 17.

Assuming that the domain boundary $x = a$ is far enough from the origin so that we can neglect the molecular potential, the solutions for $x > a$ was shown expressed in terms of Airy functions, with the resulting the boundary condition

$$\partial_x \psi(\vec{k}_\perp, a) = -(2F)^{1/3} \psi(\vec{k}_\perp, a) \alpha \frac{Ci^{+'}[-(2F)^{1/3}(a + (2W - k_\perp^2)/(2F)]}{Ci^{+}[-(2F)^{1/3}(a + (2W - k_\perp^2)/(2F)]} \tag{14}$$

Here, $\psi(\vec{k}_\perp, a)$ is the transverse Fourier transform of the wave function at $x = a$, $\vec{k}_\perp$ is the vector of transverse wavenumbers, and $Ci^+(z) = Bi(z) + iAi(z)$ is a combination of Airy functions which behaves as an outgoing wave at infinity. This expression was used to eliminate the need for an outside grid points when calculating the discrete Laplacian at the edge of the numerical grid. (This same approach was later generalized for an exact inclusion of the long-range part of the molecular potential (P11).)

The above boundary condition was utilized in conjunction with the iterative process we have developed for this kind of problems (as described in Sec. 2.3. of this report). As a result it provides the complex-valued, field-dependent value of the meta-stable energy. This, as a function of the field strength F, contains both the information about the ionization rate and about the induced nonlinear dipole. Thus, based on a non-Hermitian approach utilizing metastable electronic states, the nonlinear polarization and strong-field ionization are described together as intimately connected properties. Good agreement with the measured nonlinear index and ionization rates was shown, as illustrated in Fig. 18:

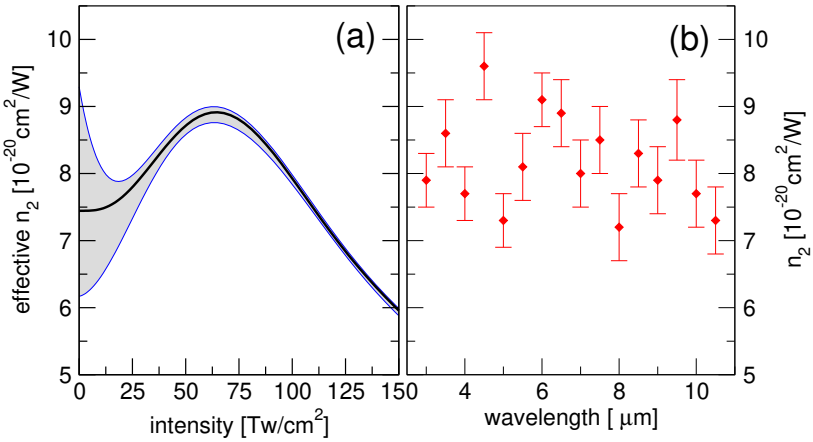

Figure 18: Effective nonlinear index as function of intensity (a) calculated from the nonlinear-dipole function. The gray area indicates the uncertainty due to different fitting functions used to represent the nonlinear dipole. Symbols (b) show the experimental results for the nonlinear index measured for a number of mid- and long-infrared wavelengths (reproduced from Ref. [43]). The vertical axes in the two panels are aligned to facilitate comparison of the measured and calculated value of the nonlinear index

Besides the nonlinear index, also the ionization rate was found in a nice agreement with the experiments. This is illustrated in Fig. 19

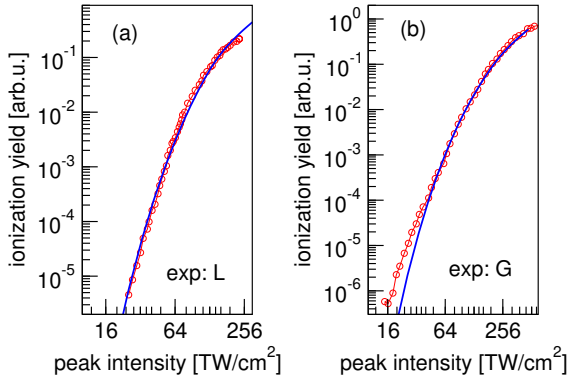

Figure 19: Ionization yield calculated for the MESA-model of O_2 (solid blue line) compared with measurements taken from two representative works, L: [44] (Lin et al.) and G: [41] (Guo et al.).

It has to be emphasized that in order to create a computational model for a *gas* of oxygen molecules, all calculations described above must be executed for every relative orientation between the molecule and the direction of the optical electric field. Subsequently, the results must be properly averaged over random molecular orientation. To make it easier to use our results in the simulation of various kind, we have developed parameterizations for the polarization and ionization aspects of the O_2 nonlinear response. With such parameterized response functions provided, large-scale simulations of infrared optical pulses interacting with gaseous media containing molecular oxygen are now possible.

The development of the molecular oxygen model was especially important, as it was the missing piece among the model based on the meta-stable electronic state approach. We have subjected the implementation to an extensive testing and at the time of this writing papers have been submitted for publication where this capability was key. One example is described in the following section.

1.3.4 Turbulence and nonlinearity in LWIR

Our capability to model the nonlinear response of both molecular nitrogen and also the recently developed oxygen opened the door to more realistic large-scale simulation of long-wavelength infrared pulse propagating in atmosphere. The crucial quality supplied by these models is in the fact that because they treat all aspects of the optical response starting from the unified quantum description, they automatically ensure the *correct proportion* between the self-focusing and de-focusing "forces" controlling the long-distance pulse propagation dynamics. This is a must especially for the long-wavelength studies, because the light-matter interactions occur at lower intensities, and over longer distances, and as such are subject to rather delicate dynamic balances between different physical effects.

With our MESA-based models for the major atmosphere constituents available, we were at last in the position to undertake investigations of the question about the mutual "interaction" between the nonlinearity of the medium and the turbulence in the context of LWIR pulse propagation.

Besides the nonlinear medium description, yet another enabling ingredient was the properly correlated description of the turbulent refractive index. For the first time to the best of our knowledge, we have developed and implemented an approach which dispenses with the traditional method based on the so-called phase screens. It was important to avoid the central assumption of the traditional method which is that the spatial scale of the turbulence is much smaller than the typical integration step used in the pulse propagation simulation. In the presence of nonlinearity and especially in the LWIR regime, this assumption breaks down. Instead, we have implemented the three-dimensional profile of the random fluctuations of the refractive index and included them as what they in fact are, namely the linear optical response of the gaseous medium. Unlike the phase-screen based method, our approach correctly preserves the isotropic nature of the fluctuations, and this is compatible with often relatively short integration step during the simulated pulse propagation. Figure 20 illustrates how the method ensures the same behavior of the index fluctuations in all directions, including the propagation direction:

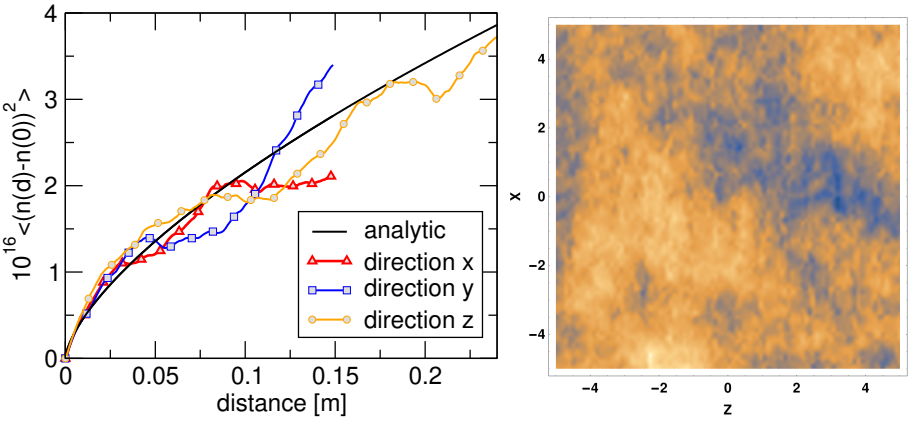

Figure 20: Turbulent model verification. Left: Correlation function $\langle[\delta n(r) - \delta n(0)]^2\rangle = C_n^2 r^{2/3}$ evaluated for r in x, y, z directions in a *single random sample* compared to the theoretical curve with the structure constant $C_n^2 = 10^{-15}\mathrm{m}^{-2/3}$. Right: Refractive index fluctuations in a 5×5cm area spanning transverse (x, vertical) and propagation (z, horizontal) directions.

This project was inspired by the experiments done in ONR MURI [34], and the parameters

of the simulation study were chosen to mimic certain characteristic such as the beam-size, peak powers, and propagation distances of tens of meters and beyond.

While our findings were in line with the earlier studies done for the NIR region (e.g. [45, 46, 47, 48]), we have found some intriguing and surprising results. As more or less expected, we could see that similar to their 800-nm wavelength counterparts, 10-micron pulses are also robust with respect to the optical turbulence. What is more surprising is that in certain aspects it appears that instead of competition, the turbulence and nonlinearity can sometimes "work together" in some kind of synergy! We have observed that the nonlinear self-trapping can be more pronounced in the presence of the turbulence. Figure 21 illustrates some of our findings; over longer distances the beam-size of the turbulent beam appears smaller than that of the ideal beam. It should be emphasized that this is in the LWIR regime which is distinct from the NIR case in that the relative size of index fluctuations and filament dimensions are different.

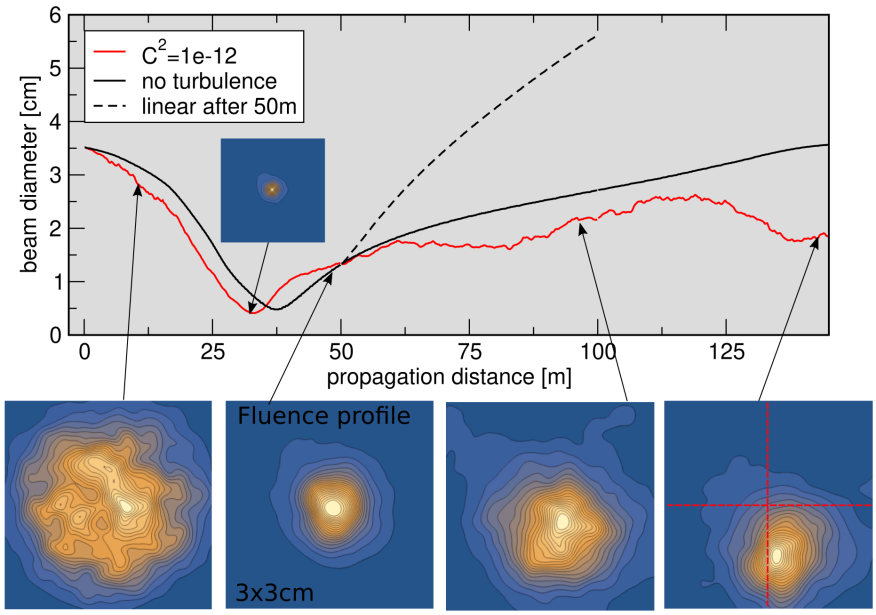

Figure 21: Nonlinear beam trapping under influence of strong turbulence. Dashes black line shown for comparison is for a pulse which propagated without nonlinearity from the fifty meter mark onward. The main result here is the red-line data representing the size of the turbulent beam, which is significantly smaller than the size of the ideal beam (shown in full black line). Red dashed cross serves as a guide to the eye to show the side ways wander of the beam.

First of all, in order to verify that the we indeed deal with the nonlinear beam self-trapping which keeps the beam from fast diffraction, we have executed a comparison run in which the nonlinearity was suddenly switched off (at the fifty-meter mark). The dashed line shows a a fast divergence, thus corroborating that it is the self-focusing nonlinearity which holds the beam size small.

Then we compared beam evolution with (red line) and without turbulence (black line) where the former shows significantly smaller, albeit fluctuating, beam diameter. The contour plots which show the transverse profile of the beam at select distances also demonstrate that while the beam is definitely deformed due to index fluctuations, it remains compact in size. Note that the beam wander is still present as is illustrated with the help of the red cross in the last beam cross-section plot.

Of course, the propagation through turbulence is random and different in every pulse-shot. To verify that the effect of improved self-trapping is not an accident, we have collected statistics shown in Fig. 22. We have repeated the simulations of the pulsed beam propagation over hundred and fifty meters of turbulent air, each with an independently randomly generated random index profile. It must be emphasized that we deal here with 3D+1 simulations which require very large numerical effort. Nevertheless, we managed to collect seventy five independent "samples" (each is a full simulation!), and obtained statistic sufficient to draw our conclusions as shown in the figure below.

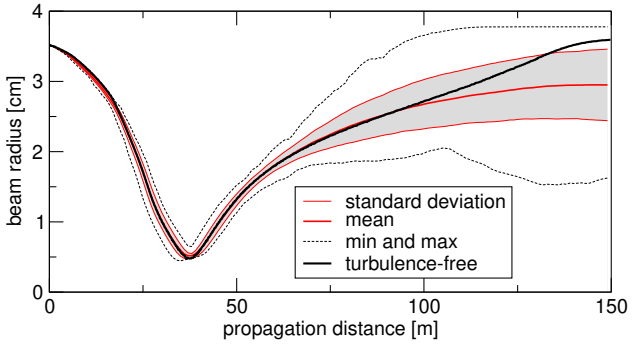

Figure 22: Nonlinear beam self-trapping with turbulence; mean beam diameter, standard deviation and minimal and maximal observed beam size versus propagation distance. On average, beam self-channeling is not hurt by the turbulence. At longer distances, typical turbulent beam is narrower than beam propagating in still air.

Thus our, results indicate that the long-wavelength infrared pulses exhibit a robustness with respect to the perturbations caused by atmospheric turbulence which is similar to that reported for near-infrared filamentation. Our comparative simulations also show that only a very strong turbulence can destroy LWIR filamentation (not illustrated in this report). Moreover, even strong turbulence does not diminish the nonlinear self-channeling. It is important to note that in the LWIR regime the beam and also the filament size can be larger than the inner scale of turbulence, hence the mechanism differs from that in near-infrared.

Surprisingly, we have obtained numerical evidence that contrary to the intuition the turbulence helps the nonlinear beam to remain spatially localized. Given the current interest in the high-power long-distance propagation of LWIR pulses, ours is a potentially significant result deserving further study.

It should be pointed out that this intriguing result would not be possible without the modeling tools developed by this project (in particular the molecular oxygen model) and the previous AFOSR-supported work by this PI (gUPPEcore simulation software). What we have here is a truly large-scale simulation which must be executed with fine resolution in all three spatial dimensions plus time, with many simulation runs repeated for statistics. It is fair to say that we are one of the few research groups that have simulation capabilities at this level.

1.3.5 Laser-acceleration of electrons

In collaboration with the group of H. Milchberg, we took on the simulation part for the work demonstrating laser wakefield acceleration of quasimonoenergetic electron bunches up to 15 MeV at

1-kHz repetition rate with 2.5-pC charge per bunch and a core with $<$7-mrad beam divergence. Acceleration was driven by 5-fs, $<$2.7-mJ laser incident on a thin, near-critical-density hydrogen gas jet. The results demonstrated the generation of high-quality electron beams from a few-cycle-pulse-driven laser plasma accelerator without the need for carrier-envelope phase stabilization.

Crucial to this experiment was the use of pulses "prepared" via their nonlinear propagation through a hollow-core waveguide (see Fig. 23) filled with Helium gas resulting in nearly circularly polarized driving pulses. Our Helium-atom model based on the universal nonlinear response theory was central to our simulations which aimed to understand the dynamics of the pulse propagation through the fiber (P10).

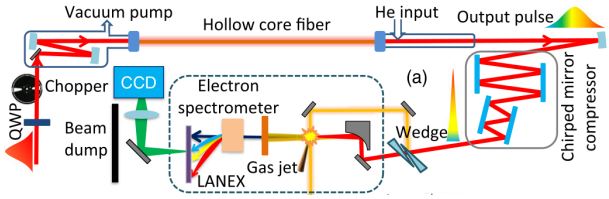

Figure 23: Electron-acceleration experiment setup (H. Milchberg group). Here the fiber filled with helium serves as a "preparatory stage" to create a pulse which is subsequently used for acceleration. Our contribution to this work was to understand via simulations the polarization dynamics of the pulse as it evolves in this fiber.

While the dynamics is very rich, it displays certain robust characteristics which our simulations allowed to discern. This is illustrated in Fig. 24 which shows the polarization dynamics of a pulse which evolves from its initially elliptic polarization at the fiber entrance to a nearly circular polarization on the output.

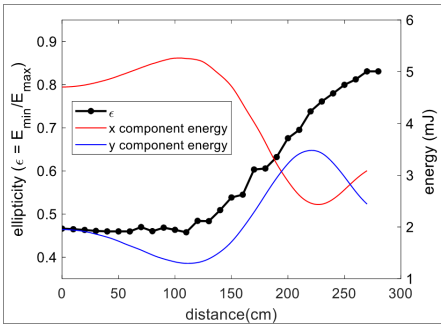

Figure 24: Propagation evolution of pulse ellipticity (black curve, left axis), $\epsilon = E_{min}/E_{max}$ for an initially elliptical polarized pulse $\epsilon = 0.47$ injected into the helium filled hollow core fibre (HCF). The red and blue curves show the energy content in horizontal and vertical components of the polarization (right axis). The evolution in the polarization state is attributed to due to the cumulative phase difference between orthogonal polarizations from weak plasma generation at the entrance, inside the HCF, and at the exit.

Our simulations showed that the circular polarization at the output from the pressure-gradient of the helium-gas in the wave guide acts as an "attractor" giving rise to nearly ideal pulses for the electron acceleration downstream from the waveguide. Moreover, we were able to infer that the mechanisms is based on the correlation between higher ionization losses in pulses which are predominantly elliptically or even linearly polarized. In comparison, a near-circularly polarized pulse suffers less from the loss due to ionization and as such it appears as dynamic "fixed point" for the polarization state.

1.3.6 Broad-band high-intensity pulse propagation for efficient high-harmonic generation

In collaboration with Zenghu Chang (UCF), we undertook an envelope pushing simulation study concerning a concept of highly-tuned two color pulses serving as a driver of extremely energetic high harmonic generation. The concept under inquiry is based on a combination of pulses with

disparate wavelength, while precisely timing they temporal overlap [49]. The idea here is that while the short-wavelength component "triggers" the strong-field ionization, the long-wavelength component is there to accelerate the freed electron to very high, keV-range energies. An example of such a pulsed waveform is in Fig. 25

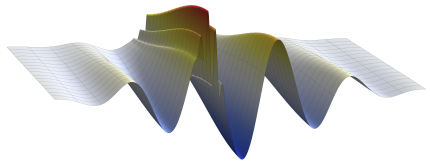

Figure 25: A combined ultrafast pulse results from the temporal overlap of two few-cycle pulses with disparate wavelengths. The longer-wavelength pulse is at $\lambda = 8\mu$m, and it is superimposed with an ultra-short-duration NIR pulse (800nm). The latter is timed such that it helps to trigger the release of the tunneling electrons. Subsequently, the electrons accelerate under the long-wavelength field, and achieve energies in the kilo-electron volt range, giving rise to extreme HHG.

Our simulations integrated the propagation dynamics of the composite pulse with the quantum-level calculations of the nonlinear response of the helium atom. As such, these simulations were exceedingly demanding, numerically. However, there was no other way to test the concept, because the outcome depends so sensitively on the minute details of the light-matter interaction. In particular, our simulation revealed a crucial role of the chromatic dispersion which can affect the relative timing of the two components of the pulse because they experience different chromatic properties of the nonlinear medium (helium in this case).

Despite the complex dynamics sensitively dependent on the properties of the medium and also on the precise parameters of the driving pulse, we were able to show that an attosecond pulse can form "spontaneously" provided parameters can be controlled. Some results are illustrated in Fig. 26

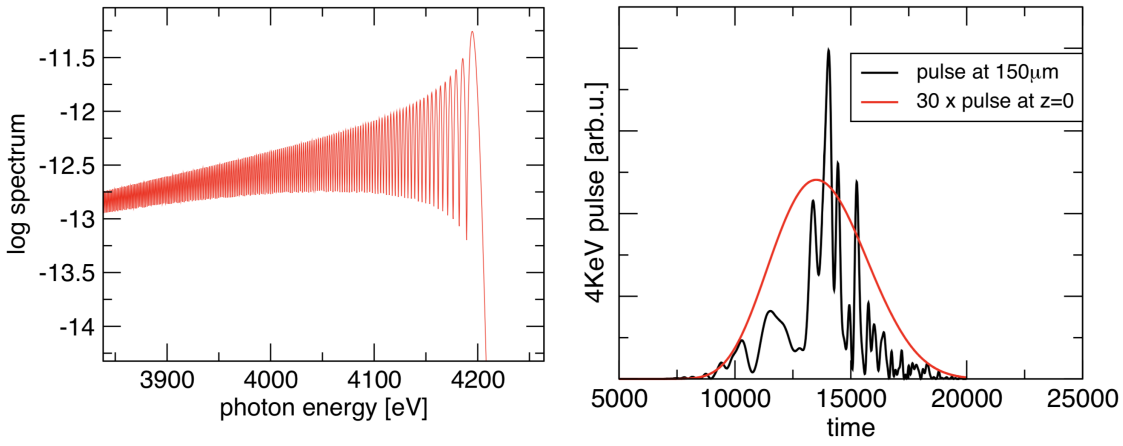

Figure 26: Simulation results for high-harmonic generation in helium gas, driven by a two-color, LW+NIR pulse (shown in the previous figure). Left: The resulting HHG spectrum extends up to its edge in the keV region. Right: Simulated propagation of the resulting attosecond pulse (time shown in thousands of atomic units). Extremely short-duration waveform forms spontaneously and experiences increase of its energy. Upon propagation over 150 micrometer gas jet its intensity grows thirty times.

So the simulations show that the intensity of a single isolated X-ray pulse in the 3.4 to 4 keV region from an 8 micron laser driven high harmonic generation can be increased between one and two orders of magnitude when a single-cycle pulse centered at 800 nm is added. At the same time, this modeling uncovered that it is not a given that a simple waveform arises from the interaction. As evident in our results, there is a complex temporal structure which indicates that the temporal coherence of the HHG radiation is less than ideal. Our numerical experiments revealed that this depends rather sensitively on both the precise timings, and on the gas density which in turn changes the tiny differences in chromatic dispersion. While they are very small, they appear to be important because of the atto-seconnd time scale of the resulting HHG pulse.

While a much more detailed study is needed to understand the dynamics in sufficient detail, our simulations already provide a proof of principle, and demonstrate that this numerical modeling can bridge the gap in time-scales between the quantum and macroscopic.

2 Impacts

2.1 Primary discipline (broadly defined light-matter interactions)

2.1.1 Broadening the application field of non-Hermitian approaches

The theme which linked different research efforts contributing to this project was the mathematics of non-Hermitian and open systems (i.e. objects or structures which exhibit some loss or strong coupling to the outside environment). While non-Hermitian methods have been used frequently in certain field of optics, their advantages were so far not recognized or fully taken advantage of in some other fields. One of the important contributions of our project is the promotion of these techniques. In particular, we have introduced these methods into nano-scaled metallic structures for the description of electron emission. We have demonstrated that our unconventional approach not only reproduced previous results, but enables something that the classical methods could not, namely a *unified description* of both the current (emitted electrons) and the nonlinear surface polarization (causing radiation at new frequencies). Thanks to our new standpoint we were able to make predictions concerning radiation properties of metallic nano-tips when irradiated by strong optical pulses.

2.1.2 New exactly solvable models

Exactly solvable models have played an indispensable role in a number of physics fields. However, for optical physics specifically it is fair to say that such models are only studied occasionally. We have developed new exactly solvable models which, generally speaking, describe a bound particle subjected to an external force which can remove this particle from the system. Not only we have introduces such toy-models, we have also developed new methods to calculate their solutions. For example, we have demonstrated combined discrete-and-continuous representations of time-dependent wave functions for tunneling particles (e.g. electrons emitted from metal structures). We trust that our demonstration of the utility of the analysis of a simplified but exactly solvable system will foster their applications in the broader optical physics.

2.1.3 Addressing fundamental questions of light matter interactions

Universality of the optical nonlinear response

The notion of universality has proven to be extremely fruitful in a number of physics disciplines. While it is mostly known from statistical physics, where it makes it possible to classify qualitatively different behaviors of complex systems in to "universality classes," ours is one of the first applications to optical physics. We have revealed that the nonlinear response of the arguably most important class of gases for nonlinear optics is in fact universal. It is universal in that different species can be described by the same framework utilizing "master functions." Master functions describe the general behavior, and the specific atom species is "selected" with only two scaling paramaters. One extremely useful consequence of this is that it essentially eliminates parameter fitting from the numerical modeling of experiments which involve noble gases exposed to strong optical pulses.

Having proposed this idea in one of our works, we went on to verify it against experimental data (this was done in a collaboration with the group of H. Milchberg in which the experiments were performed).

This work also showed the power the universlity notion adds when one has to deal with real-life experimental data which always have some levels of noise. Using our "master function" approach we demosntrated that such disturbaces can be effectively removed. Moreover, we have also shown that universlity substantially lessend the impact of the experiment callibration, thus making the whole measuremnt and its interpretation more robust.

Last but not least, the universality "angle" allowed us to implement the MESA-based description of noble gases in a way that will foster the use of these tools for the widest rage of numerical simulation in modern nonlinear optics. It always takes time for methods to be adopted by a physics community, but we are confident that we will see ours to be broadly used (in NLO) in the future.

Impact on the current debate concerning quantum tunneling dynamics

Quantum tunneling continues to fascinate physicists. Perhaps even more so recently because new experiments made it feasible to pose questions like "how much time an electron spends in the classically forbidden region of the potential barrier while it tunnels out from an atom?" There are different schools of thought about this question which concerns the very principles of the quantum theory, and the debate in the literature continues. Our work produced results that are dirrectly relevant for this unresolved problem. We have shown, using *exact results for simple models* that certain notions popular in the literature do not apply in general. In particular, we have demonstrated that in the systems we studied the particle needs finite time to emerge from the potential barrier, and this contradicts the belief that this process is instantaneous. More recently we have generalized this observation for the first time to a realistic system, namely hydrogen atom. As such our results will impact the debate and most likely tilt the future interpretations of experiments away from enforcing simple classical scenarios.

Future investigations enabled by the products of this effort

Important conceptual questions can be addressed with the tools we have created, and here we give two examples of such. The first concerns the question of the electronic optical response. While it is universally approximated as instantaneous, there is extremely little information on how fast it actually is. With the exact solution of the Stark-Coulomb system (described elsewhere in this report) it will be possible to construct time-dependent solutions for electrons responding to evolving optical fields, and directly observe in what way and how fast they react. It must be emphasized

that the high accuracy this requires precludes the current numerical methods, so this is something that one will be able to evaluate quantitatively for the first time.

Another problem which is relevant for the long-wavelength nonlinear optics with high-power pulses is the question of ionization in relatively weak fields. While it is assumed that the regime becomes approximately adiabatic and can be described with the Keldysh theory, for long wavelength there are no accurate evaluations for the post-adiabatic corrections. In this case our exact solutions to S-C Hamiltonian can be used to compare the rates in the adiabatic and non-adiabatic channels. Should the results show that the non-adiabatic corrections are never truly negligible (and our preliminary results actually show that it might be the case), the impact on the field of numerical modeling in the LWIR regime will be significant.

2.1.4 Novel numerical methods

We have developed new numerical methods specifically designed for non-Hermitian or open systems. In many situations, numerical boundaries present a challenging problem. This is especially true about open systems, because one of their features is that the escaping particles (e.g. electrons) propagate all the way to infinity, and this must be accurately reflected by the numerical method. We have designed in fact several approaches to this rather general challenge. In one of them we showed how it is possible to exactly bring the boundary conditions from infinity all the way to a close vicinity of the system we wish to model. As a result, the "size" of the underlying numerical problem shrinks dramatically.

While we have demonstrated our approach in the context of quantum theory, it is directly applicable in other fields, including optics of lossy cavities or leaky waveguides. That is why trust the methods will be applied broadly beyond the subject of this project.

2.1.5 Extensions of MESA to multielectron systems

Part of this effort was to extend the previously developed MESA (Metastable Electronic State Approach) to multielectron systems. In particular, MESA-based model for the molecular oxygen proved to present a challenge; It is inherently multi-electron system, and its molecular nature makes the previously developed treatments very difficult to apply. In a collaboration with the group of A. Becker (U. Colorado), and taking advantage of the new algorithms (as described above) we developed a new model for the unified nonlinear optical response of O_2. This impact of the result is significant, because only after finishing this step, the set of available MESA-based models now include not only the gases which are so often used in NLO, but also the major constituents of atmosphere.

2.1.6 Simulation tools for large-scale simulations of LWIR pulses in atmosphere

Finalizing the molecular oxygen model opened the door for better simulations of LWIR pulse propagation. After period of testing, we have already demonstrated the utility of these models in a truly large-scale numerical study in a collaboration with UCLA-led ONR MURI, in which we found interesting and rather surprising results concerning the interplay between nonlinearity and optical turbulence specifically in long-wavelength infrared pulses. This result is fresh, and will surely motivate further deeper studies to both understand its physical origin and to explore applications (in delivering intense radiation to distant targets in the atmosphere).

2.1.7 New exact results for an ubiquitous quantum Hamiltonian

The result with perhaps the broadest impact among the outcomes of this project is our construction of exact eigenstates for the Stark-Coulomb problem. This is a system in which a particle is exposed to an external constant force while moving in a Coulomb potential. Needless to say this is an ubiquitous situation because this combination of forces appears in essentially all single-ionizing systems. It is therefore of great interest to have an exact solution for such a system, as it will enable analytic studies as well as new numerical methods in a number of fields in optical physics and in atomic physics.

The eigenstates of this system were certainly calculated before, but only with the use of grid-based numerical approximations. What we have developed is for all practical purposes a new special function which gives the numerically exact solution for all eigenstates. Our formulation in fact provides more than one way to represent the exact solutions, and provides a great deal of analytic insight into their properties.

An important aspect of this development was our demonstration that not only it is now possible to evaluate these important eigenstates with very high or even arbitrary accuracy, but they are suitable to use them for expansions of arbitrary time dependent wave functions. To the best of our knowledge ours is the first demonstration of such an expansion which utilized *continuum-energy* bases and does this without resorting to approximations (such as quasi-discretizing the continuum).

Besides applications of this new analytic tool to various calculations in atomic physics, the result has a great educational value, too. It is one of the very rare examples where quantum state expansion is *practically* possible (i.e. beyond writing a general formula which is next-to-impossible to evaluate numerically).

We also expect that the result will attract a lot of attention in the applied mathematics community, because the formulations make it possible to study many analytic properties of these quantum states.

Last but not least, our results can be used to improve numerical methods, which deal with the Stark-Coulomb Hamiltonian, for example in the asymptotic regions away from the origin. For example, it is possible to use these states to create semi-analytic transparent boundary conditions for time-dependent simulations on discrete grid, while allowing for smaller simulation boxes.

2.2 Outreach work related to the project

An important part if this project was outreach. While it only required a small portion of time by this PI and the supported students, no additional funds were required or used. As a contribution to the college-wide effort to attract more and better American students to STEM disciplines, the PI continued his collaboration with the Basis Tucson North School. It is a college-preparatory institution which provides its student with an exceptional education in mathematics, physics, and other hard sciences. This makes it feasible and interesting to invite especially gifted students to work with us and get a taste of the real research work. This PI worked with student Howard Beck, during his junior and senior years at the Basis School. We have designed for him a guided study of a few topics related to the project. One especially successful and useful project was devoted to the rigorous description of a rigid quantum rotor as applied to the nonlinear optics of di-atomic gases in the atmosphere. As a witness to the impact of this work, this PI now uses the calculations performed by H.B. as a part of the lecture notes in his computational nonlinear optics class at the

College of Optical Sciences.

2.3 Graduate education

An important aspect of the worked performed in the framework of this project is education, and in particular STEM education. This project partially supported two students at the College of Optical Sciences and one student at the Department of Physics. Specifically, Jared Tolliver who contributed to several published works in the field of extreme nonlinear optics is a master student at the College of Optical Sciences (COS). Jonathan Heinz is PhD student at COS. He received partial support for the work on the computational methods related to open systems, and at this time he works on applications of our results in the field of optical physics. Sayedmohammad Yusofsani, also partly supported by the project, was responsible for the mathematical aspects of the theory and modeling. All three students are expected to defend their dissertations (J.H and S.Y.) and/or master report (J.T.) in the near future, and all these will be based on their research that was done as a part of this effort.

2.4 Collaborations and synergy with other projects

The ultimate goal of this project was to produce a) physics understanding and b) model implementations based on meta-stable states which will be proven as useful tools in a number of areas dealing with strong-field physics, and extreme nonlinear optics. We have utilized collaborations and connections to different project as the motivation for our development and also as a testing ground.

The theory and algorithm development in this project would be difficult if it did not build on the results from the previous AFOSR funding. We have been using the products of projects FAA9550-11-1-0144, FAA9550-13-1-0288 namely the gUPPEcore simulation suite for a number of years. It serves not only the larger computational optics group at the James Wyant College of Optical Sciences, but it continues to be utilized in several research groups.

In terms of collaborations, some of our work was done with the the University of Colorado (the group led by A. Becker), and we continue to have a fruitful collaborative relation with the University of Maryland (the group of H. Milchberg).

Outcomes of this effort were successfully used for the research utilized in the UCLA- led ONR MURI (00014-17-1-2705) where we now established and tested the ability to simulate large-scale nonlinear propagation of LWIR pulse with the help of the light-matter interaction models completed by this project (in particular the MESA-based description of molecular oxygen).

3 Dissemination of Results: Archival Publications, Invited Talks, Conference Contributions

Peer-Reviewed Publications

P12 S. Yusofsani and M. Kolesik,
Beyond FowlerNordheim model: harmonic generation from metallic nano-structures
European Physics Journal, Special Topics, https://doi.org/10.1140/epjs/s11734-021-00189-8 (2021)

P11 J. Heinz and M. Kolesik,
Transparent boundary conditions for discretized non-Hermitian eigenvalue problems
International Journal of Modern Physics C 32, 2150138, (2021)

P10 F. Salehi , M. Le , L. Railing , M. Kolesik, and H. M. Milchberg,
Laser-Accelerated, Low-Divergence 15-MeV Quasimonoenergetic Electron Bunches at 1 kHz
Physical Review X 11, 021055 (2021)

P9 J. Heinz , R. Reiff , T. Joyce, A. Becker, A. Jaron-Becker, and M. Kolesik,
Nonlinear polarization and ionization in O_2 :metastable electronic state model
Optics Express 28, 25022 (2020)

P8 S. Yusofsani and M. Kolesik,
Quantum tunneling time: Insights from an exactly solvable model
Physical Review A 101, 052121 (2020)

P7 J. Tolliver, S. Zahedpour, J. K. Wahlstrand, H. M. Milchberg, and M. Kolesik,
Nonlinearity and ionization in Xe: experiment-based calibration of a numerical model
Optics Letters 45, 5780 (2020)

P6 M. Kolesik and E. M. Wright,
Universal long-wavelength nonlinear optical response of noble gases
Optics Express 27, 25445 (2019)

P5 D. Juhasz, M. Kolesik, and P. K. Jakobsen,
Convergence and completeness for square-well Stark resonant state expansions
Journal of Mathematical Physics 59, 113501 (2018)

P4 J. Tolliver and M. Kolesik,
True versus effective Kerr nonlinear response in optical filamentation
Optics Express 26, 30172 (2018)

S1 S. Yusofsani and M. Kolesik,
Exact energy-eigenstates of the Coulomb-Stark Hamiltonian
Physical Review A, accepted

S3 S. Yusofsani and M. Kolesik,
Wigner versus Stark: Connecting Quantum to Classical in a Tunnel Ionization Process
American Journal of Physics, submitted

S2 M. Kolesik, P. Panagiotopoulos, and J.V. Moloney,
Nonlinear Localization of High Energy Long Wave Laser Pulses in Fully Correlated 3D Turbulence
Optics Letters, submitted

Invited, Keynote, and Colloquium talks presented by the PI

Colloquium: Extreme Nonlinear Optics: A computational Perspective
Dept. of Physics, University of Alabama at Birmingham
April 23, 2021

Computational Optical Physics at the Wyant College of Optical Sciences
Industrial Affiliates Workshop, Tucson Az
February 18, 2020)

Conference Presentations

15 MeV quasimonoenergetic electrons at 1 kHz with circularly polarized few-cycle pulses
Manh S Le, Fatholah Salehi, Lucas Railing, Miroslav Kolesik, Howard M Milchberg
63rd Annual Meeting of the APS Division of Plasma Physics, November 8-12, Pittsburgh, PA (2021)

4 References

References Cited

[1] L. Benassi and V. Grecchi, "Resonances in the Stark effect and strongly asymptotic approximants," *J. Phys. B: Atom. Molec. Phys.*, vol. 13, pp. 911–930, 1980.

[2] U. D. Jentschura, "Resummation of the divergent perturbation series for a hydrogen atom in an electric field," *Phys. Rev. A*, vol. 64, p. 013403, 2001.

[3] L. Mandelstam and M. Leontowitsch, "Zur theorie der schrödingerschen gleichung," *Zeitschrift für Physik*, vol. 47, pp. 131–136, Jan 1928.

[4] G. Gamow, "Zur Quantentheorie des Atomkernes," *Zeitschrift fur Physik*, vol. 51, pp. 204–212, Mar. 1928.

[5] L. A. MacColl, "Note on the transmission and reflection of wave packets by potential barriers," *Phys. Rev.*, vol. 40, pp. 621–626, May 1932.

[6] F. T. Smith, "Lifetime matrix in collision theory," *Phys. Rev.*, vol. 118, pp. 349–356, Apr 1960.

[7] M. Büttiker and R. Landauer, "Traversal time for tunneling," *Phys. Rev. Lett.*, vol. 49, pp. 1739–1742, Dec 1982.

[8] R. Landauer and T. Martin, "Barrier interaction time in tunneling," *Rev. Mod. Phys.*, vol. 66, pp. 217–228, Jan 1994.

[9] M. Büttiker, "Larmor precession and the traversal time for tunneling," *Phys. Rev. B*, vol. 27, pp. 6178–6188, May 1983.

[10] P. Eckle, M. Smolarski, P. Schlup, J. Biegert, A. Staudte, M. Schffler, H. Muller, R. Dorner, and U. Keller, "Attosecond angular streaking," *Nature Physics*, vol. 4, pp. 565 – 570, 2008.

[11] T. Zimmermann, S. Mishra, B. R. Doran, D. F. Gordon, and A. S. Landsman, "Tunneling time and weak measurement in strong field ionization," *Phys. Rev. Lett.*, vol. 116, p. 233603, Jun 2016.

[12] A. N. Pfeiffer, C. Cirelli, M. Smolarski, and U. Keller, "Recent attoclock measurements of strong field ionization," *Chemical Physics*, vol. 414, pp. 84 – 91, 2013.

[13] H. L. Cycon, R. G. Froese, W. Kirsch, and B. Simon, *Schrödinger Operators*. Springer-Verlag, 1987.

[14] U. S. Sainadh, H. Xu, X. Wang, A. Atia-Tul-Noor, W. C. Wallace, N. Douguet, A. Bray, I. Ivanov, K. Bartschat, A. Kheifets, R. T. Sang, and I. V. Litvinyuk, "Attosecond angular streaking and tunnelling time in atomic hydrogen," *Nature*, vol. 568, pp. 75–77, Apr 2019.

[15] A. S. Landsman, M. Weger, J. Maurer, R. Boge, A. Ludwig, S. Heuser, C. Cirelli, L. Gallmann, and U. Keller, "Ultrafast resolution of tunneling delay time," *Optica*, vol. 1, pp. 343–349, Nov 2014.

[16] T. Zimmermann, S. Mishra, B. R. Doran, D. F. Gordon, and A. S. Landsman, "Tunneling time and weak measurement in strong field ionization," *Phys. Rev. Lett.*, vol. 116, p. 233603, Jun 2016.

[17] U. S. Sainadh, R. T. Sang, and I. V. Litvinyuk, "Attoclock and the quest for tunnelling time in strong-field physics," *J. Phys. Photon.*, vol. 2, p. 042002, aug 2020.

[18] A. H. Larsen, U. De Giovannini, D. L. Whitenack, A. Wasserman, and A. Rubio, "Stark ionization of atoms and molecules within density functional resonance theory," *J. Phys. Chem. Lett.*, vol. 4, no. 16, pp. 2734–2738, 2013.

[19] X. M. Tong, Z. X. Zhao, and C. D. Lin, "Theory of molecular tunneling ionization," *Phys. Rev. A*, vol. 66, p. 033402, 2002.

[20] M. F. Ciappina, C. C. Chirilă, and M. Lein, "Influence of coulomb continuum wave functions in the description of high-order harmonic generation with H_2^+," *Phys. Rev. A*, vol. 75, p. 043405, Apr 2007.

[21] B. Zhang and Z.-X. Zhao, "Elliptical high-order harmonic generation from H_2^+ in linearly polarized laser fields," *Chin. Phys. Lett.*, vol. 30, p. 023202, feb 2013.

[22] M. Kolesik and E. M. Wright, "Universal long-wavelength nonlinear optical response of noble gases," *Opt. Express*, vol. 27, pp. 25445–25456, Sep 2019.

[23] L. Torlina, F. Morales, J. Kaushal, I. Ivanov, A. Kheifets, A. Zielinski, A. Scrinzi, H. G. Muller, S. Sukiasyan, M. Ivanov, and O. Smirnova, "Interpreting attoclock measurements of tunnelling times," *Nature Physics*, vol. 11, pp. 503 – 508, 2015.

[24] H. Ni, U. Saalmann, and J.-M. Rost, "Tunneling ionization time resolved by backpropagation," *Phys. Rev. Lett.*, vol. 117, p. 023002, Jul 2016.

[25] H. Ni, U. Saalmann, and J.-M. Rost, "Tunneling exit characteristics from classical backpropagation of an ionized electron wave packet," *Phys. Rev. A*, vol. 97, p. 013426, Jan 2018.

[26] M. T. Hassan, T. T. Luu, A. Moulet, O. Raskazovskaya, P. Zhokhov, M. Garg, N. Karpowicz, A. M. Zheltikov, V. Pervak, F. Krausz, and E. Goulielmakis, "Optical attosecond pulses and tracking the nonlinear response of bound electrons," *Nature*, vol. 530, pp. 66–70, 2016.

[27] M. Krüger, M. Schenk, M. Förster, and P. Hommelhoff, "Attosecond physics in photoemission from a metal nanotip," *Journal of Physics B: Atomic, Molecular and Optical Physics*, vol. 45, p. 074006, mar 2012.

[28] S. Varro and F. Ehlotzky, "High-order multiphoton ionization at metal surfaces by laser fields of moderate power," *Phys. Rev. A*, vol. 57, 01 1998.

[29] M. Schenk, M. Krüger, and P. Hommelhoff, "Strong-field above-threshold photoemission from sharp metal tips," *Phys. Rev. Lett.*, vol. 105, p. 257601, 2010.

[30] A. Couairon and A. Mysyrowicz, "Femtosecond filamentation in transparent media," *Phys. Rep.*, vol. 441, no. 2-4, pp. 47–189, 2007.

[31] A. Bahl, J. K. Wahlstrand, S. Zahedpour, H. M. Milchberg, and M. Kolesik, "Nonlinear optical polarization response and plasma generation in noble gases: Comparison of metastable-electronic-state-approach models to experiments," *Phys. Rev. A*, vol. 96, p. 043867, 2017.

[32] M. Kolesik and E. Wright, "Universal long-wavelength nonlinear optical response of noble gases," *Optics express*, vol. 27, no. 18, pp. 25445–25456, 2019.

[33] H. M. Milchberg, Y.-H. Chen, Y.-H. Cheng, N. Jhajj, J. P. Palastro, E. W. Rosenthal, S. Varma, J. K. Wahlstrand, and S. Zahedpour, "The extreme nonlinear optics of gases and femtosecond optical filamentationa)," *Physics of Plasmas*, vol. 21, no. 10, 2014.

[34] S. Tochitsky, E. Welch, M. Polyanskiy, I. Pogorelsky, P. Panagiotopoulos, M. Kolesik, E. M. Wright, S. W. Koch, J. V. Moloney, J. Pigeon, and C. Joshi, "Megafilament in air formed by self-guided terawatt long-wavelength infrared lase," *Nature Photonics*, vol. 13, p. 41, 2019.

[35] S.-D. Liang, *Quantum Tunneling and Field Electron Emission Theories*. World Scientific Publishing Co., 2014.

[36] R. H. Fowler and L. Nordheim, "Electron emission in intense electric fields," *R. Soc. Lond*, vol. 119, May 1928.

[37] J. W. Gadzuk and E. W. Plummer, "Field emission energy distribution," *Rev. Mod. Phys.*, vol. 45, p. 487, 1973.

[38] C. C. Wu, K. L. Ou, and C. L. Tseng, "Fabrication and characterization of well-aligned and ultra-sharp silicon nanotip array," *Nanoscale Res. Lett.*, vol. 7, p. 120, 2012.

[39] S. Han, H. Kim, Y. W. Kim, Y.-J. Kim, S. Kim, I.-Y. Park, and S.-W. Kim, "High-harmonic generation by field enhanced femtosecond pulses in metal-sapphire nanostructure," *Nature Communications*, vol. 7, 2016.

[40] M. Kolesik and E. M. Wright, "Universal long-wavelength nonlinear optical response of noble gases," *Opt. Express*, vol. 27, pp. 25445–25456, Sep 2019.

[41] C. Guo, M. Li, J. P. Nibarger, and G. N. Gibson, "Single and double ionization of diatomic molecules in strong laser fields," *Phys. Rev. A*, vol. 58, pp. R4271–R4274, 1998.

[42] M. Nesrallah, A. Hakami, G. Bart, C. R. McDonald, C. Varin, and T. Brabec, "Measuring the kerr nonlinearity via seeded kerr instability amplification: conceptual analysis," *Opt. Express*, vol. 26, pp. 7646–7654, Mar 2018.

[43] S. Zahedpour, S. W. Hancock, and H. M. Milchberg, "Ultrashort infrared 2.5-11μm pulses: spatiotemporal profiles and absolute nonlinear response of air constituents," *Opt. Lett.*, vol. 44, no. 4, pp. 843–846, 2019.

[44] Z. Lin, X. Jia, C. Wang, Z. Hu, H. Kang, W. Quan, X. Lai, X. Liu, J. Chen, B. Zeng, W. Chu, J. Yao, Y. Cheng, and Z. Xu, "Ionization suppression of diatomic molecules in an intense midinfrared laser field," *Phys. Rev. Lett.*, vol. 108, p. 223001, 2012.

[45] M. H. Helle, G. DiComo, S. Gregory, A. Mamonau, D. Kaganovich, R. Fischer, J. Palastro, S. Melis, and J. Peñano, "Beating optical-turbulence limits using high-peak-power lasers," *Phys. Rev. Applied*, vol. 12, p. 054043, 2019.

[46] G. DiComo, M. Helle, D. Kaganovich, A. Schmitt-Sody, J. Elle, and J. Peñano, "Nonlinear self-channeling of high-power lasers through controlled atmospheric turbulence," *J. Opt. Soc. Am. B*, vol. 37, pp. 797–803, Mar 2020.

[47] D. Eeltink, N. Berti, N. Marchiando, S. Hermelin, J. Gateau, M. Brunetti, J. P. Wolf, and J. Kasparian, "Triggering filamentation using turbulence," *Phys. Rev. A*, vol. 94, p. 033806, 2016.

[48] B. Hafizi, J. R. Peñano, J. P. Palastro, R. P. Fischer, and G. DiComo, "Laser beam self-focusing in turbulent dissipative media," *Opt. Lett.*, vol. 42, pp. 298–301, Jan 2017.

[49] Z. Chang, "Enhancing kev high harmonic signals generated by long-wave infrared lasers," *OSA Continuum*, vol. 2, p. 2131, 2019.

[50] O. Smirnova and M. Ivanov, *Multielectron High Harmonic Generation: Simple Man on a Complex Plane*, ch. 7, pp. 201–256. John Wiley & Sons, Ltd, 2014.

[51] M. Lewenstein, P. Balcou, M. Y. Ivanov, A. L'Huillier, and P. B. Corkum, "Theory of high-harmonic generation by low-frequency laser fields," *Phys. Rev. A*, vol. 49, pp. 2117–2132, Mar 1994.

5 Changes

6 Technical updates